ACSNANO

www.acsnano.org

ARTICLE

Modulating Plaque Inflammation *via* Targeted mRNA Nanoparticles for the Treatment of Atherosclerosis

Mingzhu Gao, Maoping Tang, William Ho, Yilong Teng, Qijing Chen, Lei Bu, Xiaoyang Xu,* and Xue-Qing Zhang*

Cite This: *ACS Nano* 2023, 17, 17721−17739

Read Online

ACCESS | Metrics & More | Article Recommendations | Supporting Information

ABSTRACT: **Atherosclerosis is a common pathology present in many cardiovascular diseases. Although the current therapies (including statins and inhibitors of the serine protease PCSK9) can effectively reduce low-density lipoprotein (LDL) cholesterol levels to guideline-recommended levels, major adverse cardiovascular events still occur frequently. Indeed, the subendothelial retention of lipoproteins in the artery wall triggers multiple events of inflammation in macrophages and is a major contributor to the pathological progression of atherosclerosis. It has been gradually recognized that modulating inflammation is, therefore, an attractive avenue to forestall and treat atherosclerosis and its complications. Unfortunately, challenges with specificity and efficacy in managing plaque inflammation have hindered progress in atherosclerosis treatment. Herein, we report an NP-mediated mRNA therapeutic approach to target atherosclerotic lesional macrophages, modulating inflammation in advanced atherosclerotic lesions for the treatment of atherosclerosis. We demonstrated that the targeted NPs containing *IL-10* mRNA colocalized with M2-like macrophages and induced IL-10 production in atherosclerotic plaques following intravenous administration to Western diet (WD)-fed *Ldlr*$^{-/-}$ mice. Additionally, the lesions showed a significantly alleviated inflammatory response, as evidenced by reduced oxidative stress and macrophage apoptosis, resulting in decreased lipid deposition, diminished necrotic areas, and increased fiber cap thickness. These results demonstrate the successful delivery of mRNA therapeutics to macrophage-enriched plaques in a preclinical model of advanced atherosclerosis, showing that this targeted NP inflammation management approach has great potential for translation into a wide range of clinical applications.**

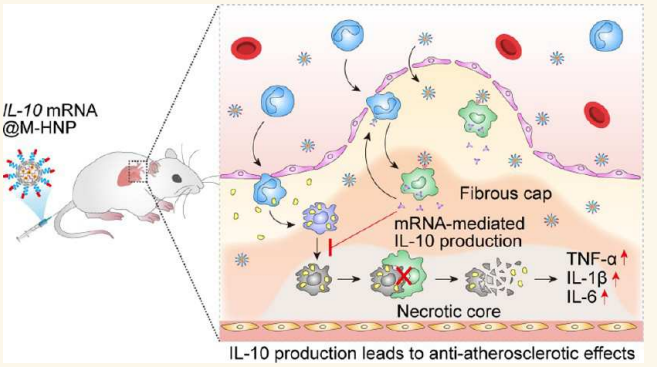

KEYWORDS: *mRNA, inflammation-resolving IL-10, targeted nanoparticles, lesional macrophages, atherosclerosis*

INTRODUCTION

The progressive worsening of atherosclerotic lesions into unstable plaques gives rise to acute luminal thrombosis and adverse cardiovascular events, leading to myocardial infarction (MI), unstable angina, sudden death from coronary heart disease, and stroke.[1] Over the past three decades, statins and cholesterol absorption inhibitors (*e.g.*, PCSK9 inhibitors) that reduce the levels of LDL have consistently been considered the treatment of choice for atherosclerosis.[2,3] However, the current LDL-lowering therapies do not adequately address the residual cardiovascular risk which is derived from the underlying inflammation, and thus, atherosclerosis still remains a major cause of morbidity and mortality.[3−5]

Recent evidence has revealed that atherosclerotic plaques develop through a macrophage-driven, maladaptive inflammatory response to subendothelial retention of apolipoprotein B-containing lipoproteins.[4] This maladaptive response leads to defects in inflammation resolution that manifests as defective clearance of apoptotic cells and egress of inflammatory cells, persistent oxidative stress and inflammatory state, and eventually, unstable plaques vulnerable to rupture are formed, triggering thrombosis and MI.[6] This pathological process highlights inflammation as an attractive target in the treatment

Received: February 1, 2023
Accepted: August 30, 2023
Published: September 5, 2023

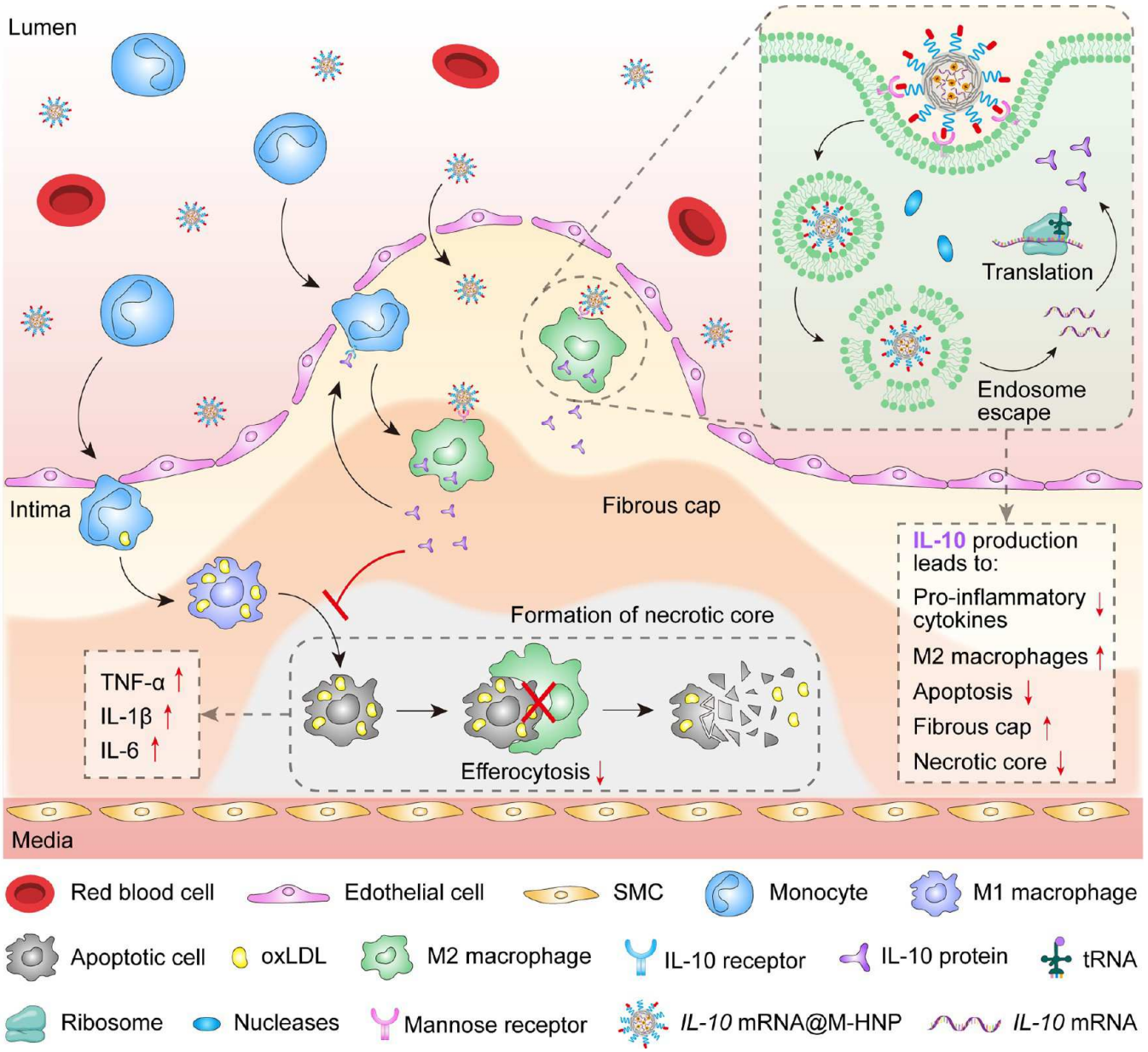

Figure 1. Schematic illustration of the NP-aided specific delivery of *IL-10* mRNA to atherosclerotic lesional macrophages for enhanced resolution of inflammation. *IL-10* mRNA-loaded M-HNPs enter dysfunctional intima *via* leaky endothelial junctions followed by active targeting of M2-like macrophages located in the fibrous cap surrounding the lipid core of plaques through mannose receptor-mediated interaction, which together facilitate NP accumulation within atherosclerotic plaques. The internalized NPs escape from endosomes, release therapeutic mRNA, and subsequently induce the expression of IL-10 in M2 macrophages. The secreted IL-10 effectively inhibits the expression of pro-inflammatory cytokines, such as tumor necrosis factor-α (TNF-α), interleukin-1β (IL-1β), and interleukin-6 (IL-6), promoting inflammation resolution. The elevated expression level of IL-10 also drives polarization of macrophages toward M2 phenotypes, diminishes cell apoptosis and necrotic area in atherosclerotic lesions, and increases fibrous cap thickness, which results in a potent antiatherosclerotic effect.

of atherosclerosis; however, the development of anti-inflammatory drugs (including canakinumab and colchicine) is hampered by immunosuppressive adverse events accompanied by systemic use.[3,7] As such, there is an unmet need to develop therapies that can precisely and safely modulate inflammation within the local plaque microenvironment to combat atherosclerotic vascular diseases, providing complementary benefits in conjunction with LDL-reducing therapies.

Herein, we present a targeted mRNA therapeutic approach: an atherosclerotic lesional macrophage-targeting nanoparticle (NP) delivering an anti-inflammatory mRNA, Interleukin-10 (IL-10), promotes the resolution of inflammation in advanced atherosclerotic lesions to halt the progress of atherosclerosis. IL-10 is a potent resolving mediator produced predominantly by macrophages that plays an important role in the resolution of inflammation and tissue repair within the local atherosclerotic lesion.[8,9] IL-10 is also known to exert a multifaceted protective effect against atherosclerotic lesion formation by modulating lipid metabolism in macrophages, along with its antiatherogenic role in inhibiting the production of pro-inflammatory cytokines, MMPs, ROS, and apoptosis.[10] Although IL-10 has shown a promising protective role in

https://doi.org/10.1021/acsnano.3c00958
ACS Nano 2023, 17, 17721−17739

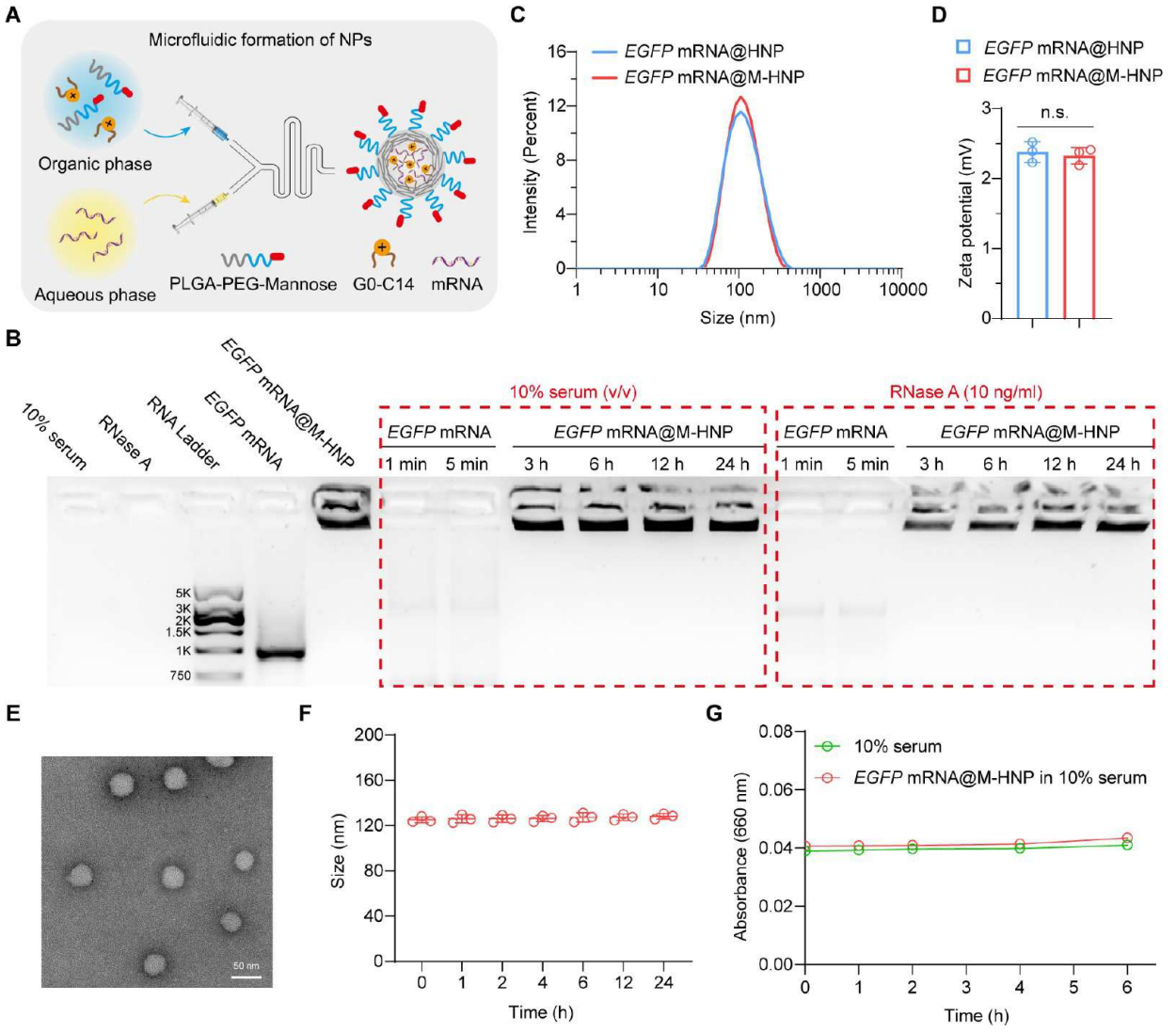

Figure 2. Preparation and characterization of mRNA NPs. (A) Schematic diagram of mRNA NP design and self-assembly *via* a modified microfluidic-based method. (B) Stability of naked mRNA and NP-encapsulating mRNA against serum and RNase. (C and D) The size and zeta potential of *EGFP* mRNA@HNPs and *EGFP* mRNA@M-HNPs were evaluated by DLS (n = 3). (E) TEM images of *EGFP* mRNA@M-HNPs. Scale bars, 50 nm. (F) *EGFP* mRNA@M-HNPs diameters was assessed by DLS in 10% serum condition at 37 °C for 0, 1, 2, 4, 6, 12, and 24 h (n = 3). (G) Turbidity of *EGFP* mRNA@M-HNPs in 10% serum at 37 °C for 0, 1, 2, 4, and 6 h was measured by a microplate reader at the absorbance of 660 nm (n = 3). All data are shown as means ± SD, and statistical significance was determined using a two-tailed Student's t test. n.s., not significant.

atherogenesis, limited success has been achieved in the translation from bench to bedside due to its short plasma half-life (~3 min) and rapid clearance, making it difficult to reach and maintain therapeutic drug concentrations at the site of inflammation for desired effects.[11,12] We hypothesize that targeted delivery of mRNA encoding IL-10 (*IL-10* mRNA) to macrophage-rich plaques could be a promising approach for resolving atherosclerotic plaque inflammation while addressing formulation and delivery challenges encountered with protein-based therapeutics.

In vitro transcribed (IVT) mRNA has emerged as a versatile class of drug, being used in vaccines to therapeutics, due to its potential to produce any protein of interest.[13] To fully harness the potential of mRNA-based therapy, delivery vehicles capable of specifically transferring mRNA to the diseased organs and cells are critically needed.[14] A variety of NP platforms have been explored to circumvent delivery barriers for mRNA, including rapid blood clearance, nuclease degradation, poor cellular internalization, and endosomal escape.[15−17] However, most of the developed NPs preferentially target mRNA to the liver and spleen following systemic delivery, which significantly limits the clinical use of mRNA-based therapies.[18] As a result, despite the success of SARS-CoV-2 mRNA vaccines, no mRNA-based protein replacement therapy has been approved.

Considerable efforts have been made to develop tissue- or cell-targeted delivery systems;[19,20] however, NP platforms that allow selective transfer of therapeutic mRNA to lesional macrophages have yet to be explored. This work provides a proof-of-concept for the design and preclinical evaluation of targeted NPs that can specifically deliver mRNA encoding therapeutic IL-10 to lesional macrophages for resolving inflammation (Figure 1). We constructed NPs using our previously reported cationic lipid-like molecule (designated G0-C14) and a biodegradable poly(lactide-*co*-glycolide)-*b*-poly(ethylene glycol) (PLGA-PEG) diblock copolymer through microfluidic self-assembly methods.[21] Macrophages,

https://doi.org/10.1021/acsnano.3c00958
ACS Nano 2023, 17, 17721−17739

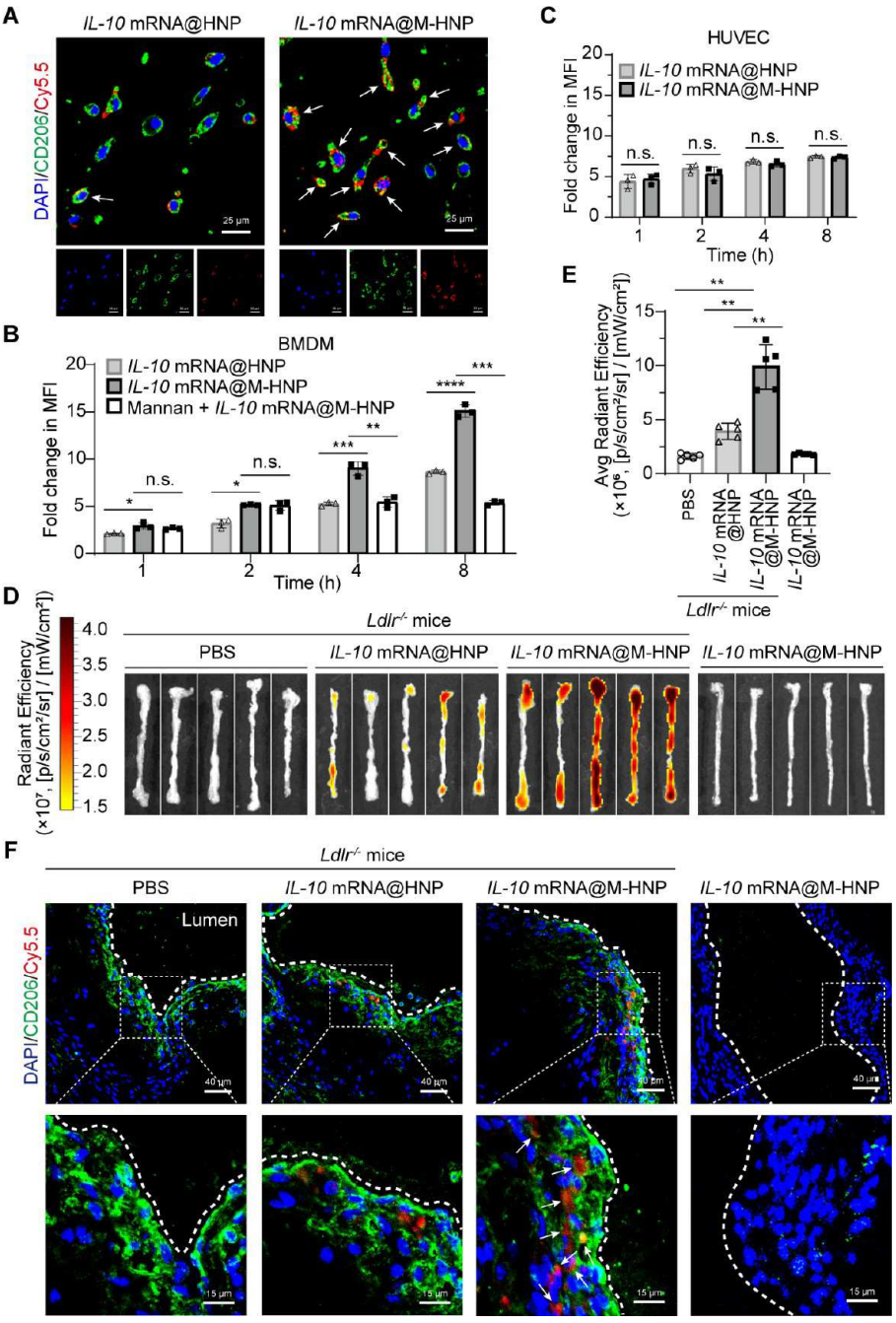

Figure 3. Uptake of *IL-10* mRNA-loaded NPs in BMDMs and NP localization in aorta of mice postintravenous injection. (A) CLSM images of IL-4-stimulated BMDMs after incubation with Cy5.5-labeled NPs (red) for 4 h. Nuclei were stained with DAPI (blue), and BMDMs were immunostained with CD206 (green). White arrows indicate the colocalization of NPs with CD206-positive cells. Scale bar, 25 μm. (B and C) Uptake efficiency of Cy5.5-labeled NPs in BMDMs (B) and HUVECs (C) (n = 3). IL-4-stimulated BMDMs or HUVECs were treated with NPs for 1, 2, 4, and 8 h and mean fluorescence intensity (MFI) of cells was analyzed by flow cytometry. IL-4-induced BMDMs were pretreated with mannan followed by incubation with *IL-10* mRNA@M-HNPs for 1, 2, 4, and 8 h and MFI of cells was analyzed (B). The MFI of IL-4-stimulated BMDMs or HUVECs (without NP treatment) was used as the baseline value. Statistical significance was determined using a two-tailed Student's t test. (D) IVIS imaging of aortas collected at 24 h from the healthy mice or 12-week WD-fed $Ldlr^{-/-}$ mice after intravenous injection with PBS or Cy5.5-labeled NPs. (E) Quantification analysis of fluorescence signal in aortas by Living Image 4.5 software (n = 5). Statistical significance was determined using one-way ANOVA. (F) Immunofluorescence analysis of the colocalization of Cy5.5-labeled NPs (red) and $CD206^{+}$ macrophages (green) in the aortic root. Nuclei were stained with DAPI (blue). White arrows indicate the colocalization of NPs with CD206. Scale bar, 15 μm. All data are shown as mean ± SD *P < 0.05, **P < 0.01, ***P < 0.001, ****P < 0.0001. n.s., not significant.

especially the M2 polarized macrophages, are known to localize to the fibrous cap surrounding the lipid core of plaques and express high levels of mannose receptor (CD206), making them attractive targets for atherosclerosis diagnosis and treatment.[22,23] Encouraged by this, we functionalized NP surfaces with mannose to impart a targeting capability to the G0-C14/PLGA-PEG hybrid NPs (M-HNPs). Using a WD-fed $Ldlr^{-/-}$ mouse model of atherosclerosis, our results show that

https://doi.org/10.1021/acsnano.3c00958
ACS Nano 2023, 17, 17721−17739

the *IL-10* mRNA-loaded M-HNPs (*IL-10* mRNA@M-HNPs) tend to accumulate within the macrophage-rich region of atherosclerotic plaques following intravenous (iv) injection, inducing IL-10 production. These NPs promote resolution of inflammation, inhibit oxidative stress and apoptosis, and exert antiatherosclerotic effects by reducing lipid deposition and size of necrotic areas and increasing fiber cap thickness. Our findings demonstrate the use of selective delivery of mRNA to produce the potent inflammation-resolving mediator IL-10 within macrophage-rich plaques, which shows enormous promise for combating atherosclerosis. Our approach also provides insights into the management of localized inflammation with translational potential for addressing many related conditions.

RESULTS

Synthesis and Characterization of Macrophage-Targeting NPs Loaded with mRNA. As shown in Figure 2A, a facile self-assembly method was employed to prepare the targeted mRNA NPs consisting of the following two components: (i) mannose-conjugated PLGA-PEG (PLGA-PEG-Mannose, Figure S1) that is capable of increasing plasma circulation time and facilitating plaque accumulation and (ii) a self-synthesized cationic lipid-like material termed G0-C14 (Figure S2). G0-C14 was incorporated due to its capabilities to complex with mRNA *via* electrostatic interaction and to self-assemble with PLGA-PEG-Mannose to form stable NPs (M-HNPs). An agarose gel retardation assay was performed to study the electrostatic interaction between G0-C14 and mRNA encoding enhanced green fluorescent protein (*EGFP* mRNA). Retardation of mRNA migration in electrophoresis occurred at a G0-C14/mRNA mass ratio of 20 or above, suggesting a strong mRNA binding of G0-C14 (Figure S3). We then prepared the NPs at a G0-C14/mRNA weight ratio of 30 and did not observe any mRNA leaching, as evidenced by electrophoresis (Figure 2B), which suggested that mRNA was effectively encapsulated within the NPs. Additionally, after incubation with 10% fetal bovine serum (FBS) or RNase, mRNA degraded rapidly in its free form but exhibited resistance to degradation over a period of 24 h when encapsulated within NPs.

The hydrodynamic size and zeta potential of targeted *EGFP* mRNA@M-HNPs (122.1 ± 1.1 nm, 2.33 ± 0.12 mV) were similar to that of nontargeted *EGFP* mRNA@HNPs (125.2 ± 0.6 nm, 2.38 ± 0.22 mV) as characterized by dynamic light scattering (DLS), indicating that incorporation of the mannose moiety on the surface has no significant effect on the particle size and zeta potential (Figure 2C,D). The spherical and uniform morphologies of the targeted *EGFP* mRNA@M-HNPs were characterized by transmission electron microscopy (TEM) (Figure 2E). The stability of the *EGFP* mRNA@M-HNPs was also examined by monitoring particle size in the presence of serum at 37 °C, and no significant change was observed in this *in vivo* like condition over 24 h (Figure 2F). There is no serum-induced aggregation, as evidenced by turbidity measurement (Figure 2G). These results suggest that the developed M-HNPs have a stable and rigid nanostructure that can protect the encapsulated mRNA.

Cellular Uptake of M-HNPs by Macrophages. We used IL-4-activated bone marrow-derived macrophages (BMDMs) and RAW 264.7, both of which display M2-like phenotype,[24,25] to evaluate *in vitro* targeting efficacy of Cy5.5-labeled M-HNPs or HNPs loaded with *IL-10* mRNA. *IL-10* mRNA was synthesized *in vitro* using a T7 RNA polymerase-mediated transcription reaction (Figure S4 and Table S1). The fluorescence assay demonstrated that *IL-10* mRNA was successfully encapsulated into HNPs or M-HNPs, with encapsulation efficiencies of 92.3% and 92.8%, respectively. The integrity of *IL-10* mRNA extracted from NPs was confirmed by capillary electrophoresis (Figure S5). The hydrodynamic size and zeta potential of *IL-10* mRNA-loaded NPs were found to be similar to those of *EGFP* mRNA-loaded NPs (Figure S6). There was no significant change in the particle size of *IL-10* mRNA@M-HNPs after incubation with serum at 37 °C for 24 h, which further confirmed the stability of the mRNA-encapsulated M-HNPs under *in vivo* like conditions (Figure S7). NP uptake in IL-4-activated BMDMs was enhanced by increasing the percentage of incorporated mannose moiety and reached the maximum value when PLGA-PEG was completely replaced by the mannose-conjugated copolymer (Figure S8). In addition, confocal laser scanning microscope (CLSM) images showed that more *IL-10* mRNA@M-HNPs colocalized with CD206 expressed on the cell surface than nontargeted *IL-10* mRNA@HNPs (Figure 3A and Figure S9A). We also noted that cellular uptake of *IL-10* mRNA@M-HNPs in RAW 264.7 cells was substantially inhibited in the presence of mannan, which blocks mannose binding to CD206, thus indicating mannose receptor-mediated endocytosis (Figure S9B).

NP cellular internalization was also quantitatively analyzed in BMDMs and human umbilical vein endothelial cells (HUVECs) by flow cytometry. As shown in Figure 3B, a higher intensity of Cy5.5 signal was detected in BMDMs treated with *IL-10* mRNA@M-HNPs than in the cells treated with *IL-10* mRNA@HNPs, and the magnitude of enhancement in NP uptake dramatically increased along with incubation time. Additionally, uptake of *IL-10* mRNA@M-HNPs by BMDMs was markedly reduced by the treatment with mannan, which is likely due to the blockage of mannose receptors (Figure 3B). As expected, we did not observe any enhancement in cellular uptake of *IL-10* mRNA@M-HNPs in HUVECs that do not express CD206 (Figure 3C). These results suggest that NP uptake in BMDMs was significantly enhanced by mannose conjugation. Both CLSM images and flow cytometry showed that the *IL-10* mRNA@M-HNPs were internalized by RAW 264.7 cells in a time- and dose-dependent manner (Figure S9C–F). Taken together, these results reveal that the ligand–receptor interaction plays a key role in the macrophage uptake of *IL-10* mRNA@M-HNPs.

***In Vivo* Evaluation of Targeting Efficiency of M-HNPs to Atherosclerotic Lesions.** We determined the pharmacokinetic properties of our NP platform *in vivo*. C57BL/6 mice were intravenously injected with an equivalent dose of Cy5-labeled mRNA encoding Firefly Luciferase (Cy5-*Luc* mRNA) in naked or NP forms. The results demonstrated that free mRNA was rapidly cleared following iv injection with a circulation half-life of around 17 min, whereas the circulation half-life of mRNA encapsulated within NPs was significantly extended to nearly 2 h (Figure S10). Both targeted M-HNPs and nontargeted HNPs have similar circulation profiles.

We then investigated the capability of the NPs to target atherosclerotic lesions *in vivo*. Cy5.5-labeled M-HNPs or HNPs that encapsulated an equivalent dose of *IL-10* mRNA were intravenously injected into a WD-fed $Ldlr^{-/-}$ mouse model of atherosclerosis. Aorta tissues and major organs (including heart, liver, spleen, lung, and kidney) were

https://doi.org/10.1021/acsnano.3c00958
ACS Nano 2023, 17, 17721–17739

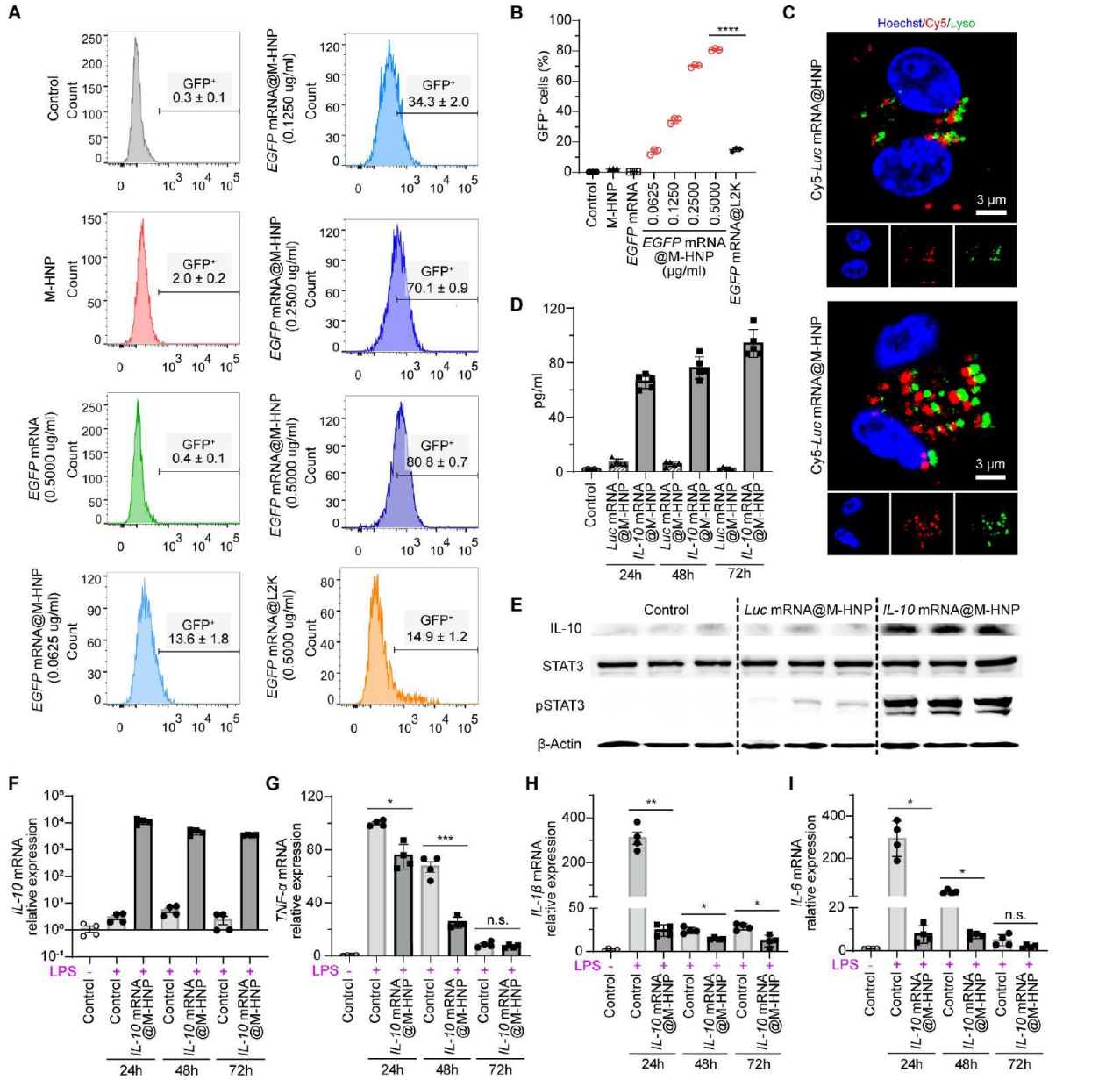

Figure 4. Transfection efficiency and anti-inflammatory effects of *IL-10* mRNA@M-HNPs. (A) Histogram analysis of the *in vitro* transfection efficiency in BMDMs by flow cytometry. (B) The percentage of GFP-positive cells in BMDMs was assessed using FlowJo software (n = 3). Statistical significance was determined using a two-tailed Student's t test. (C) CLSM images of BMDMs at 4 h after incubation with NPs incorporated with Cy5-labeled *Luc* mRNA (red). Nuclei were stained with Hoechst 33342 (blue), and endosomes were stained with LysoTracker Green (green). Scale bar, 3 μm. (D) ELISA analysis for IL-10 levels in BMDMs treated with *Luc* mRNA@M-HNPs or *IL-10* mRNA@M-HNPs for 24, 48, or 72 h (n = 3). (E) Western blotting of IL-10, STAT3, and pSTAT3 in BMDMs treated with PBS, *Luc* mRNA@M-HNPs, or *IL-10* mRNA@M-HNPs for 24 h. β-Actin was used as a housekeeping standard (n = 3). (F–I) qRT-PCR analysis for *IL-10* (F), *TNF-α* (G), *IL-1β* (H), and *IL-6* (I) levels in BMDMs, which were pretreated with *IL-10* mRNA@M-HNPs for 6 h and were stimulated by LPS for 24, 48, or 72 h. Untreated BMDMs were used as the negative control, and LPS-only treatment was used as the positive control (n = 4). All data are shown as means ± SD, and statistical significance was determined using one-way ANOVA (*P < 0.05, **P < 0.01, ***P < 0.001, ****P < 0.0001). n.s., not significant.

harvested 24 h following injection and measured for Cy5 fluorescence signals using an In-Vivo Imaging System (IVIS). In *Ldlr*$^{-/-}$ mice, the fluorescence signal in aorta tissues treated with *IL-10* mRNA@M-HNPs was about 3-fold higher than in *IL-10* mRNA@HNP-treated tissues. In contrast, no fluorescence signal was observed in the aorta of healthy mice treated with *IL-10* mRNA@M-HNPs (Figure 3D,E). Immunofluorescence staining of cryo-sectioned aortic roots also demonstrated that the incorporation of mannose moieties markedly increased NP accumulation within the lesion area of the aortic root (Figure 3F). Abundant colocalization of *IL-10* mRNA@M-HNPs with the CD206^{+} lesion area was observed in the aortic root sections from *Ldlr*$^{-/-}$ mice, which is attributed to the fact that the majority of M2-like macrophages are present in the fibrous cap surrounding the lipid-rich core of plaques and express a high level of CD206.[23] The results indicate that both prolonged blood circulation and ligand-mediated active targeting facilitate the homing of the mRNA-loaded M-HNPs

https://doi.org/10.1021/acsnano.3c00958
ACS Nano 2023, 17, 17721−17739

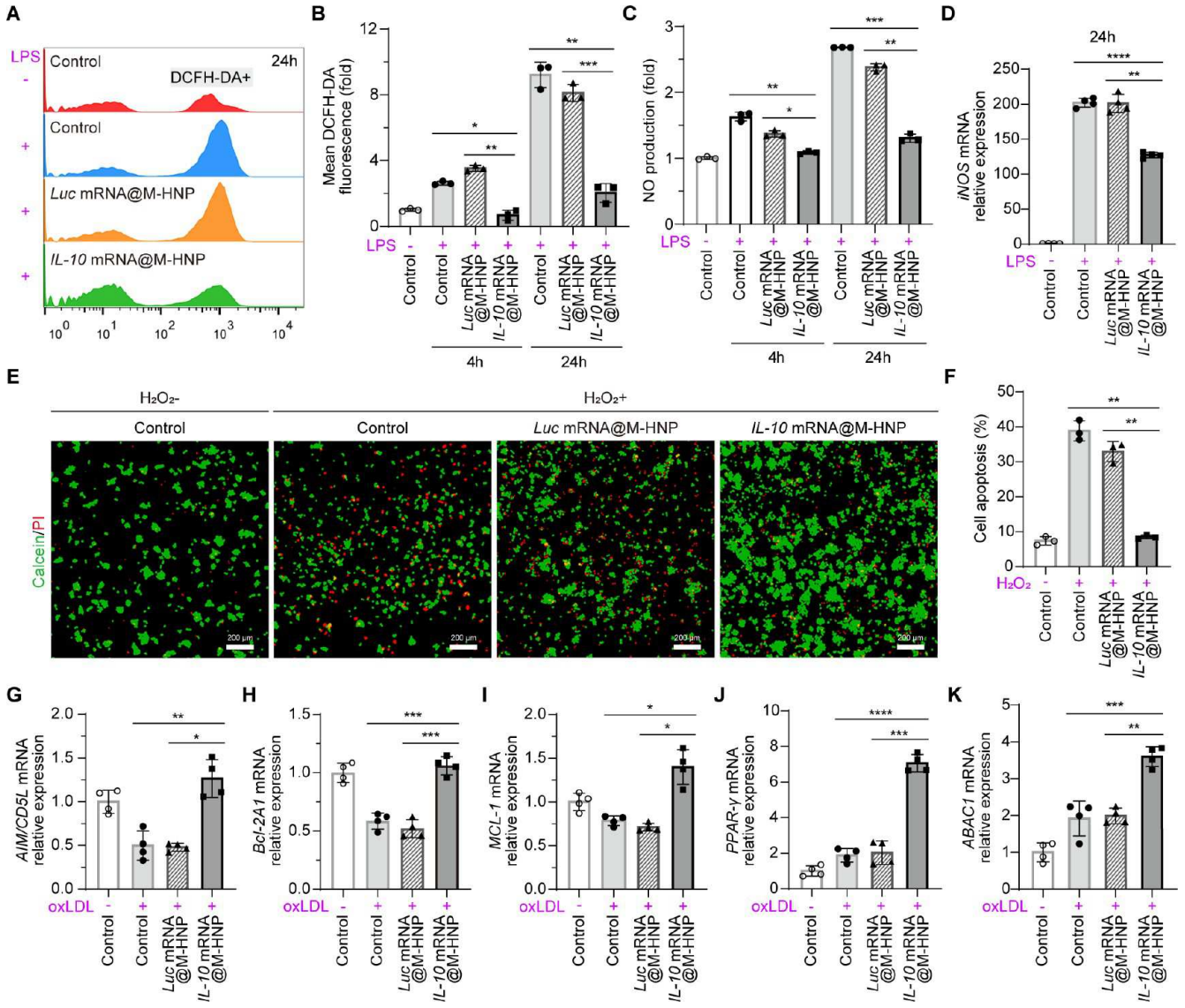

Figure 5. ***IL-10*** **mRNA@M-HNPs inhibit oxidative stress and apoptosis and regulate lipid metabolism in BMDMs. (A) BMDMs were treated with PBS,** ***Luc*** **mRNA@M-HNPs, or** ***IL-10*** **mRNA@M-HNPs for 6 h followed by 24 h of LPS stimulation, and generation of ROS was then analyzed by flow cytometry. DCFH-DA was used as a probe for ROS generation. (B) Histogram analysis of ROS generation for 4 or 24 h after LPS stimulation, using FlowJo software (*n* = 3). ROS levels of untreated BMDMs were used as the baseline for normalization. (C) NO production in BMDMs after 4 or 24 h of LPS stimulation (*n* = 3). These BMDMs were pretreated with PBS,** ***Luc*** **mRNA@M-HNPs, or** ***IL-10*** **mRNA@M-HNPs for 6 h. NO levels of untreated BMDMs were used as the baseline for normalization. (D) qRT-PCR analysis for** ***iNOS*** **level of BMDMs (*n* = 4). (E) Fluorescence images showing apoptosis of BMDMs pretreated with PBS,** ***Luc*** **mRNA@M-HNPs, or** ***IL-10*** **mRNA@M-HNPs for 6 h and then exposed to H_2O_2 for 30 min. Cells were stained with Calcein (green)/PI (red) apoptosis detection reagent. Scale bar, 200 μm. (F) Histogram analysis of apoptosis by flow cytometry (*n* = 3). (G−K) Relative mRNA expression levels of antiapoptosis genes** ***AIM/CD5L*** **(G),** ***Bcl-2A1*** **(H), and** ***MCL-1*** **(I) and lipid metabolism genes** ***PPAR-γ*** **(J) and** ***ABAC1*** **(K) in oxLDL-induced BMDMs with different treatments (*n* = 4). Untreated BMDMs were used as the negative control. All data are shown as means ± SD, and statistical significance was determined** ***via*** **one-way ANOVA (**P* < 0.05, ***P* < 0.01, ****P* < 0.001, *****P* < 0.0001).**

to atherosclerotic lesions, leading to enhanced plaque accumulation. Since the liver and kidney are major organs responsible for drug metabolism and elimination, NP accumulation is expected in these two organs (Figure S11). There is no significant difference in fluorescence signals between organs from the *IL-10* mRNA@M-HNP-treated group and the *IL-10* mRNA@HNP-treated group. Our finding is consistent with previous studies that NPs with small size are prone to accumulate in the liver, kidney, and spleen following systemic administration.[26]

In Vitro **Assessment of M-HNP-Mediated mRNA Transfection.** Macrophages are usually considered as hard-to-transfect cells since they have evolved to recognize foreign nucleic acids and they are highly differentiated.[27] Here, we conducted *in vitro* transfection experiments in BMDMs and RAW264.7 cells using *EGFP* mRNA as a reporter mRNA and determined the transfection efficiency by measuring GFP-positive cells in the entire cell population using flow cytometry. Cells were transfected with commonly used Lipofectamine 2000 (L2K) as a positive control, and less than 15% of the treated cells displayed a positive fluorescence signal at an

https://doi.org/10.1021/acsnano.3c00958
ACS Nano 2023, 17, 17721−17739

mRNA concentration of 0.5 μg/mL (Figure 4A,B and Figure S12). Compared with L2K, M-HNPs showed significantly higher transfection efficiency (Figure S13) and also exhibited an mRNA dose-depend increase. 80.8% and 70.2% of GFP-positive cells were detected respectively in BMDMs and RAW264.7 cells treated with the highest mRNA concentrations of 0.5 μg/mL (Figure 4A,B, and Figure S12). Since endosomal escape is crucial for effective mRNA delivery, we monitored intracellular trafficking of the NPs loaded with Cy5-*Luc* mRNA to assess the endosomal escape ability of our NP platform. Figure 4C and Figure S14 demonstrated that the internalized Cy5-*Luc* mRNA mainly localized within endosomes after 1 h of incubation and escaped from the endosomes following incubation with cells for 4 h, suggesting NP-assisted release of mRNA into the cytoplasm.

We then transfected BMDMs using M-HNPs loaded with *IL-10* mRNA to examine the IL-10 expression and anti-inflammatory effects. IL-10 levels from the supernatants of cells treated with *IL-10* mRNA@M-HNPs were detected by ELISA. The results as shown in Figure 4D indicated that the cumulative secretion of IL-10 protein increased with time, up to 72 h. Western blot analysis of cell lysates demonstrated that *IL-10* mRNA@M-HNPs elicited the expression of the IL-10 protein in BMDMs (Figure 4E). No IL-10 production was detected in the culture supernatants or cell lysates from the control or *Luc* mRNA@M-HNP groups (Figure 4D,E). We investigated whether the IL-10/signal transducer and activator of transcription 3 (STAT3) axis is involved in the pathways through which IL-10 exerts anti-inflammatory effects. As shown in Figure 4E, compared to the control or *Luc* mRNA-loaded NP treatment, *IL-10* mRNA@M-HNPs treatment induced significant phosphorylation of STAT3, implying successful activation of STAT3 by IL-10. Quantitative reverse transcription PCR (qRT-PCR) results also confirmed elevated *IL-10* mRNA expression after *IL-10* mRNA@M-HNPs treatment as shown in Figure 4F. Substantial levels of the target gene expression could be still detected 3 days after NP treatment (Figure 4F). Taken together, these results indicate that the developed M-HNPs could mediate the efficient cytosolic delivery of mRNA, leading to prolonged translation of the mRNA encoding IL-10 in macrophages.

Assessment of Anti-inflammatory Effects. Pro-inflammatory cytokines, such as TNF-α, IL-1β, and IL-6, are considered to be major mediators responsible for the inflammatory-immunological pathomechanism of atherosclerosis, and their elevation results in complex effects on multiple signaling pathways involved in lipid processing and plaque formation.[28] Suppression of these pro-inflammatory cytokines has been shown to provide multiple therapeutic benefits in atherosclerosis.[29] In the next set of experiments, we evaluated whether the *IL-10* mRNA@M-HNPs were able to alter the lipopolysaccharide (LPS)-induced inflammatory response in BMDMs. Isolated BMDMs were pretreated for 6 h with *IL-10* mRNA@M-HNPs followed by LPS stimulation to induce a pro-inflammatory response. Cells cultured with the medium alone or the medium containing LPS served as control groups. As shown in Figure 4G−I, LPS treatment promoted the production of TNF-α, IL-1β, and IL-6 in macrophages, and *IL-10* mRNA@M-HNPs substantially suppressed their secretion, revealing that the expressed IL-10 retains its bioactivity and exerts a potent anti-inflammatory effect. It is worth noting that NP treatment significantly inhibited the production of atherogenic factors TNF-α, IL-1β, and IL-6 up to 48 h post LPS stimulation, suggesting an intense and prolonged anti-inflammatory response. Although the LPS-induced inflammation attenuated drastically at 72 h post LPS stimulation, a slight reduction in the levels of these atherogenic cytokines was still observed in the NP-treated cells, which is consistent with the duration of *IL-10* mRNA translation in macrophages. More importantly, no obvious cytotoxicity was observed in cells at 12 or 24 h after NP treatment at all tested concentrations, implying excellent biocompatibility of *IL-10* mRNA@M-HNPs (Figure S15).

ROS-Scavenging and Antiapoptotic Activities of *IL-10* mRNA@M-HNPs in Macrophages. Under normal physiological conditions, there is a dynamic balance between reactive oxygen species (ROS) production and the antioxidant defense system that constitutes cellular redox homeostasis.[30] However, overproduction of ROS will disrupt the redox homeostasis, which initiates an amplification of inflammatory responses, thus resulting in oxidative stress and tissue injury.[31] Here, we examined whether the developed *IL-10* mRNA@M-HNPs can suppress the LPS-induced ROS generation in BMDMs. LPS stimulation induced a high 2′,7′-dichlorofluorescin diacetate (DCFH-DA) fluorescence signal (Figure 5A,B), implying the generation of high levels of intracellular ROS. The intracellular levels of ROS increased with the LPS stimulation time. By contrast, *IL-10* mRNA@M-HNPs significantly reduced LPS-induced ROS production by ∼78% and 75% over untreated control and *Luc* mRNA@M-HNPs, respectively, at 24 h after LPS challenge (Figure 5A,B).

At the atherosclerotic plaque, overproduced NO reacts with ROS to form peroxynitrite (ONOO−) which subsequently interacts with biomolecules such as lipids, DNA, and proteins to cause oxidative endothelial injury, contributing to the pathogenesis of acute cardiovascular events.[32] Therefore, for atherosclerosis therapy, it is crucial to prevent peroxynitrite generation at the inflammation site by controlling NO production in macrophage cells. Twenty-four h of LPS stimulation led to a ∼2.7-fold higher NO level in BMDMs compared to control cells without any treatment (Figure 5C), whereas the LPS-induced NO production decreased by ∼51% in the cells pretreated with *IL-10* mRNA-loaded M-HNPs. Additionally, we noted that pretreatment with *IL-10* mRNA@M-HNPs resulted in a significant reduction in the mRNA levels of *inducible nitric oxide synthase* (*iNOS*) in the LPS-challenged BMDMs (Figure 5D), which led to inhibition of NO generation. On the other hand, pretreatment with M-HNPs lacking *IL-10* mRNA (*e.g.*, *Luc* mRNA@M-HNPs) could not suppress either ROS or NO generation in LPS-activated macrophages.

Continuous overproduction of ROS causes oxidation of lipids, DNA, and proteins, ultimately inducing cell apoptosis.[33] In this context, we examined the protective effects of *IL-10* mRNA@M-HNPs on H_2O_2-induced cell apoptosis in BMDMs using a Calcein-AM/PI live/dead staining assay. Immunofluorescence microscopy and flow cytometry data showed that pretreatment with *IL-10* mRNA-loaded M-HNPs resulted in many fewer apoptotic (PI positive) cells compared to untreated control and *Luc* mRNA@M-HNPs (Figure 5E,F). After pretreatment with *IL-10* mRNA@M-HNPs, the survival rate of H_2O_2-insulted BMDMs was restored to the basal level measured in cells cultured with medium alone (Figure 5F). We subsequently assayed the intracellular mRNA levels of three well-known macrophage survival proteins: apoptosis inhibitor in macrophages (AIM/CD5L), Bcl-2A1, and MCL-1 in

https://doi.org/10.1021/acsnano.3c00958
ACS Nano 2023, 17, 17721−17739

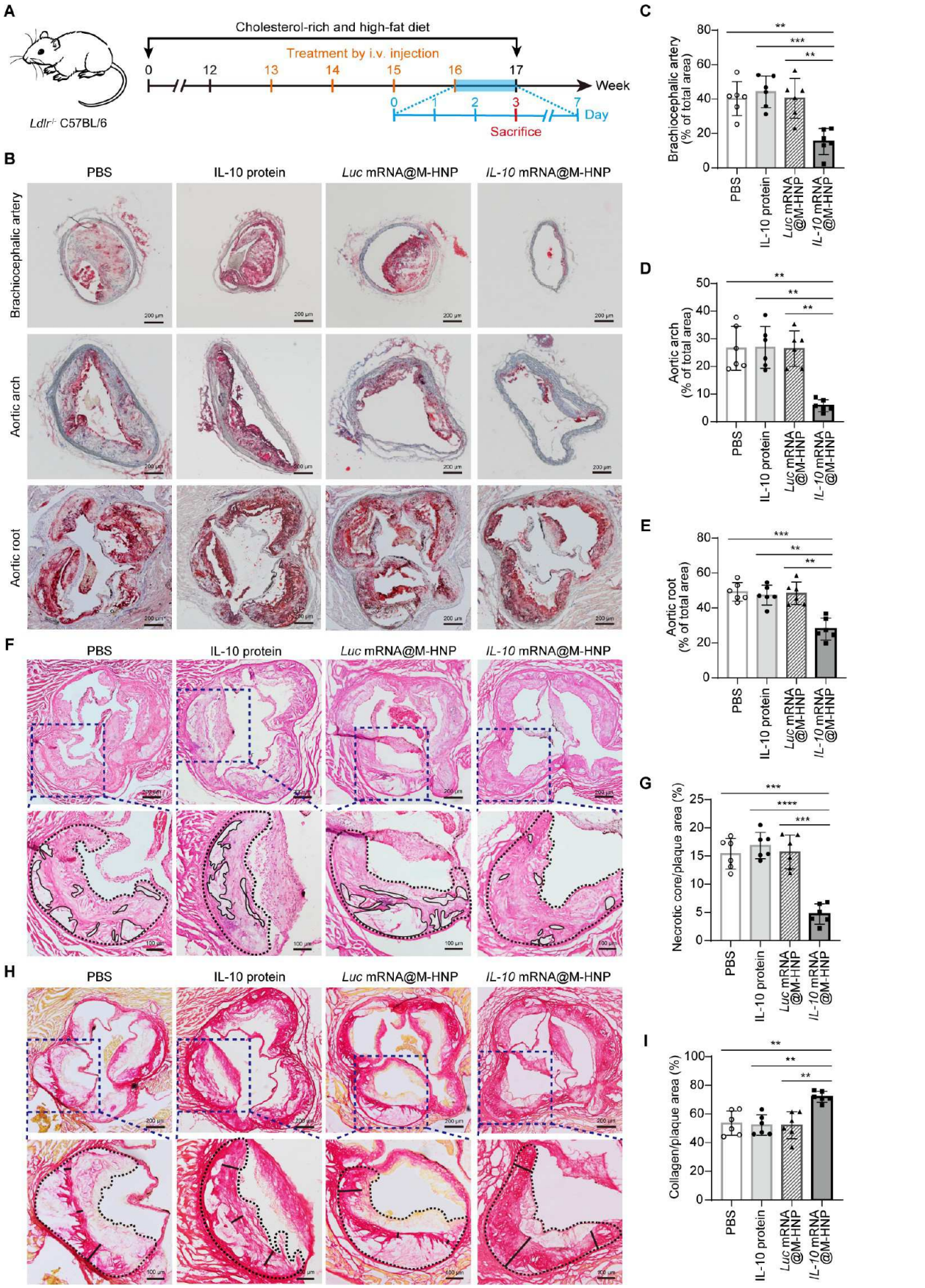

Figure 6. WD-fed *Ldlr*$^{-/-}$ mice treated with *IL-10* mRNA@M-HNPs display a prominent reduction of atherosclerotic lesion and necrotic core areas and a significant increase in collagen cap thickness. (A) Schematic illustration of the establishment of atherosclerosis and treatment regimen in *Ldlr*$^{-/-}$ mice. Samples were collected on the third day after the last injection for analysis. (B) ORO staining of

https://doi.org/10.1021/acsnano.3c00958
ACS Nano 2023, 17, 17721−17739

Figure 6. continued

brachiocephalic artery, aortic arch, and aortic root cryosections in *Ldlr*$^{-/-}$ mice with indicated treatments. Scale bar, 200 μm. (C−E) Quantitative analysis of the relative plaque area in sections of the brachiocephalic artery (C), aortic arch (D), and aortic root (E) (n = 6). (F) H&E staining of the aortic root sections from *Ldlr*$^{-/-}$ mice with indicated treatments. The black dotted lines and black solid lines indicate the plaque area and the necrotic core, respectively. Scale bar, 200 μm. (G) Quantitative analysis of the necrotic core relative to plaque area by ImageJ software (n = 6). (H) Picrosirius red staining of the aortic root sections from *Ldlr*$^{-/-}$ mice with indicated treatments. Collagen cap thickness was measured at the midpoint and shoulder region of each plaque. Scale bar, 200 μm. (I) Quantitative analysis of the collagen cap thickness relative to plaque area by ImageJ software (n = 6). All data are shown as means ± SD and statistical significance was determined using one-way ANOVA (*P < 0.05, **P < 0.01, ***P < 0.001, ****P < 0.0001).

BMDMs. The basal levels of the three mRNAs were decreased when exposed to oxidized LDL (oxLDL) but were markedly increased by *IL-10* mRNA@M-HNPs treatment (Figure 5G−I). Notably, *IL-10* mRNA@M-HNPs also upregulated the expression levels of *PPAR-γ* and *ABCA1*, two key genes involved in the cholesterol efflux pathway, in the oxLDL-induced senescent foamy macrophages (Figure 5J,K). These results imply that *IL-10* mRNA@M-HNPs suppress ROS-induced BMDM apoptosis and promote cholesterol efflux through the upregulation of the PPAR-γ/ABCA1 pathway, thus offering antiatherogenic benefits.

Antiatherosclerotic Effects of Targeted NPs Incorporating *IL-10* mRNA in *Ldlr*$^{-/-}$ Mice. Atherosclerosis does not tend to be clinically symptomatic until the formation of vulnerable plaques consisting of necrotic cores with distinct fibrous caps.[28] Due to this, patients usually receive medical treatment after advanced atherosclerosis is already established and clinical syndromes are detectable. For these reasons, we investigated the therapeutic efficacy of targeted delivery of *IL-10* mRNA in a mouse model of atherosclerosis, where treatment began after relatively stable lesions were established and continued as the disease progressed to vulnerable plaques.

Ldlr$^{-/-}$ mice were fed a Western-type high-fat/high-cholesterol diet for 16 weeks to develop advanced atherosclerotic plaques. At week 13, mice were intravenously injected with different treatments twice a week for 4 weeks and sacrificed at week 17 (Figure 6A). On the third day after the last injection, we conducted histological analysis to examine hallmarks associated with advanced atherosclerotic plaques from the whole aorta, brachiocephalic arteries, aortic arches, and aortic roots. As shown in Figure 6B and Figure S16, the tissues were stained by Oil Red O (ORO) and the resultant red region indicates plaque area. After 16 weeks on the WD, mice treated with PBS (plaque areas of ∼26%, ∼40%, ∼26%, and ∼49% of the total tissue area), IL-10 protein (∼23%, ∼44%, ∼27%, and ∼47%), or *Luc* mRNA@M-HNPs (∼25%, ∼41%, ∼26%, and ∼48%) showed large plaque areas in the whole aorta, brachiocephalic artery, aortic arch, and aortic root sections (Figure 6C−E and Figure S16). Interestingly, *IL-10* mRNA@M-HNP treatment significantly decreased plaque area down to ∼4%, ∼15%, ∼6%, and ∼28% of the total tissue area in whole aorta, brachiocephalic artery, aortic arch, and aortic root sections, respectively. Hematoxylin & eosin (H&E) staining on the cryosections of aortic roots showed that lesions from PBS, IL-10 protein, or *Luc* mRNA@M-HNP control group were predominantly composed of lipid-rich necrotic cores. Compared to the control groups, the *IL-10* mRNA@M-HNP group exhibited a notable reduction in both necrotic core area and the ratio of necrotic core area to lesion size (Figure 6F,G). In parallel, Picrosirius red staining demonstrated a significantly higher content of collagen around plaques in the group treated with *IL-10* mRNA@M-HNPs, indicating an enhanced fibrous cap thickness (Figure 6H,I). These results collectively demonstrate that the plaque macrophage-targeted M-HNPs containing *IL-10* mRNA exert potent antiatherosclerotic effects by reducing necrotic core size, thickening the cap, stabilizing the plaque, and facilitating enhanced resolution of inflammation.

Study of the Antiatherosclerotic Mechanism. We further tested expression of IL-10 and major pro-inflammatory cytokines in aortic roots and serum of *Ldlr*$^{-/-}$ mice with atherosclerosis to address mechanisms underlying the anti-atherosclerotic effects of *IL-10* mRNA@M-HNPs. Immunofluorescence staining results showed that only the aortic sections from the group treated with M-HNPs exhibited bright fluorescence signals corresponding to IL-10 in the lesional area, and no visible signals were observed in the lesions of mice treated with PBS or *Luc* mRNA@M-HNPs (Figure 7A,B). The ELISA assay further indicated a significant increase in IL-10 expression in the aortic tissues and serum of mice treated with *IL-10* mRNA@M-HNPs compared to the two control groups (Figures S17 and S18A). Both PBS and *Luc* mRNA@M-HNP treatment resulted in strong fluorescence signals corresponding to TNF-α, IL-1β, and IL-6 in the aortic root sections, implying the presence of an inflammatory environment in the atherosclerotic lesion (Figure 7A). In contrast, treatment with *IL-10* mRNA@M-HNPs significantly inhibited the production of pro-inflammatory cytokines in the plaques (Figure 7C−E). Meanwhile, there was a notable reduction in serum levels of IL-1β and IL-6 in mice subjected to *IL-10* mRNA@M-HNP treatment (Figure S18B,C). Dihydroethidium (DHE) staining was also conducted to evaluate ROS levels in the sectioned aortic roots, brachiocephalic arteries, and aortic arches collected from atherosclerotic mice. Both observation and quantitative analysis of the sectioned aortic roots revealed that red fluorescence of ethidium, an indicator of oxidative stress, was markedly attenuated after treatment with *IL-10* mRNA@M-HNPs when compared with that of PBS or *Luc* mRNA@M-HNP treatment (Figure 7F,G). Similarly, substantially reduced levels of oxidative stress were observed in the sectioned brachiocephalic arteries and aortic arches of mice treated with *IL-10* mRNA@M-HNPs compared with those of the two control groups (Figure S19). Aortic root sections were stained and analyzed by immunofluorescence imaging for TUNEL^{+} (terminal deoxynucleotidyl transferase-mediated deoxyuridine triphosphate nick-end-labeling-positive) apoptotic cells. The results demonstrated that *IL-10* mRNA@M-HNP treatment resulted in a significant 2.5-fold decrease in the apoptosis rates over either PBS or *Luc* mRNA@M-HNP (Figure 7H,I).

Matrix metallopeptidase 9 (MMP-9), a collagen-degrading metalloproteinase secreted by inflammatory macrophages, has been shown to be an independent predictor of atherosclerotic plaque instability in coronary heart disease patients.[34] It has

https://doi.org/10.1021/acsnano.3c00958
ACS Nano 2023, 17, 17721−17739

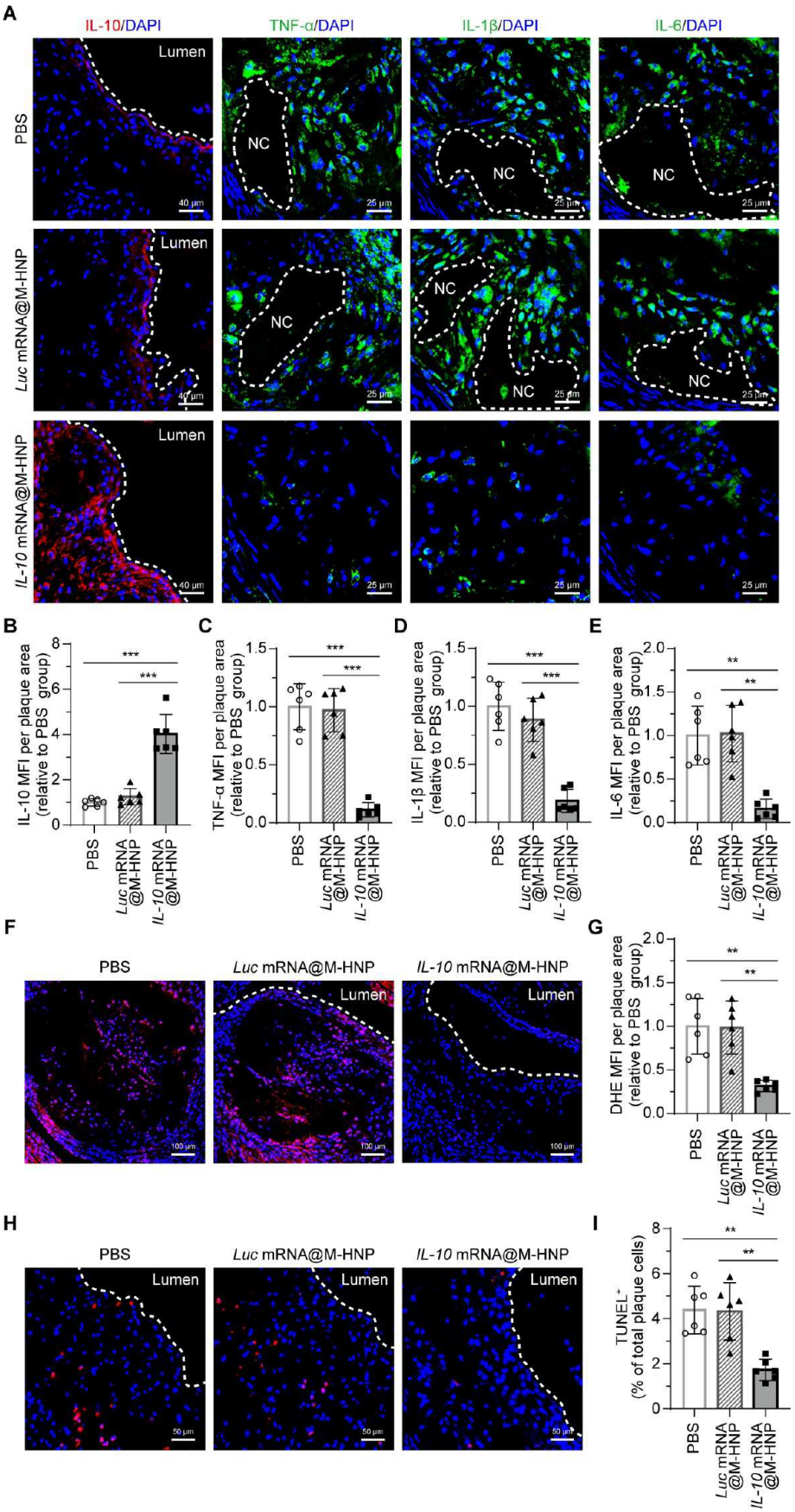

Figure 7. ***IL-10*** **mRNA@M-HNP treatment decreases inflammation, oxidative stress, and apoptosis in WD-fed** $Ldlr^{-/-}$ **mice. (A) Immunofluorescence staining of the inflammatory cytokines IL-10 (red), TNF-α (green), IL-1β (green), and IL-6 (green) in the aortic root of** $Ldlr^{-/-}$ **mice with indicated treatments. Nuclei were stained with DAPI (blue). The necrotic core (NC) is framed by a white dashed line.**

https://doi.org/10.1021/acsnano.3c00958
ACS Nano 2023, 17, 17721−17739

Figure 7. continued

Scale bar, 25 μm. (B–E) MFI quantification of IL-10 (B), TNF-α (C), IL-1β (D), and IL-6 (E) on the aortic root sections, normalized to the PBS group (n = 6). (F) DHE staining of aortic root sections for superoxide (red) in $Ldlr^{-/-}$ mice with the indicated treatments. Nuclei were stained with DAPI (blue). Scale bar, 100 μm. (G) MFI quantification of superoxide, normalized to the PBS group (n = 6). (H) TUNEL staining of aortic root sections for apoptotic cells (red) from mice treated as indicated. Nuclei were stained with DAPI (blue). Scale bar, 50 μm. (I) Quantitative analysis of apoptotic cells shown in (H) relative to the total number of plaque cells (n = 6). All data are shown as means ± SD, and statistical significance was determined using one-way ANOVA (*P < 0.05, **P < 0.01, ***P < 0.001, ****P < 0.0001).

been reported that elevated expression of MMP-9 is associated with the increased size of the necrotic core of unstable atherosclerotic plaques.[35] Immunohistochemical staining of aortic roots showed that the MMP-9 expression level was significantly reduced in the lesions of *IL-10* mRNA@M-HNP-treated mice (Figure S20A,B), which is one of the reasons causing the increased fibrous cap thickness. The ratios of lesion-resident macrophage or smooth muscle cell number to overall lesion area were similar among all treatment groups (Figure S20C and D), implying that the beneficial effects of *IL-10* mRNA@M-HNPs were not mediated by decreasing these cells in lesions. Mice treated with *IL-10* mRNA@M-HNPs had considerably higher levels of CD206 expression in their aortic root lesions than did the other control groups. Immunofluorescence results revealed a higher number of CD206-positive cells in the aortic root sections of mice treated with *IL-10* mRNA@M-HNPs compared with the two control groups (Figure S21). In addition, notable red fluorescence signals corresponding to pSTAT3 were observed within the CD206-positive area of aortic root sections in mice treated with *IL-10* mRNA@M-HNPs, indicating the activation of Janus kinase 1 (JAK1)/STAT3 signaling pathway in the majority of M2-polarized macrophages (Figure S22). These findings suggest that efficient expression of IL-10 in atherosclerotic lesions mediated by NP delivery of *IL-10* mRNA leads to enhanced resolution of inflammation as well as decreased oxidative stress and cell apoptosis. Collectively, this approach may represent a promising treatment strategy for patients with atherosclerosis.

***In Vivo* Safety Evaluation.** Next, we investigated possible side effects in healthy C57BL/6 mice after 4 weeks of treatment with *IL-10* mRNA@M-HNPs with two injections per week. The mice were sacrificed under euthanasia 3 days after the last injection, and hearts, livers, spleens, lungs, kidneys, brains, and blood were harvested to evaluate the safety profile of the *IL-10* mRNA-loaded M-HNPs. As shown in Figure S23, we observed no significant differences in body weight or organ coefficient among all of the treatment groups. Additionally, no obvious signs of injury were detected in the H&E-stained organs of each treatment group (Figure 8A). There were also no significant differences in a series of hematological and biochemical parameters, including red blood cell count (RBC), white blood cell count (WBC), hemoglobin (HGB), hematocrit (HCT), mean corpuscular volume (MCV), mean corpuscular hemoglobin (MCH), mean corpuscular hemoglobin concentration (MCHC), lymphocytes, alanine aminotransferase (ALT), aspartate aminotransferase (AST), total protein (TP), albumin (ALB), triglycerides (TG), low-density lipoprotein (LDL), total cholesterol (TC), creatinine (Crea), urea nitrogen (BUN), and glucose (Glu) (Figure 8B).

In vivo safety of *IL-10* mRNA@M-HNPs was also confirmed by the aforementioned $Ldlr^{-/-}$ mice model in histological, blood biochemical, and hematological end points after 4 weeks of NPs treatment with two injections per week (Table S2 and Figures S24 and S25). In contrast to the two control groups, the plasma lipid profile in the *IL-10* mRNA@M-HNP treatment group exhibited slightly lower levels of TC, TG, and LDL (Figure S24E–G). We observed a low level of fat accumulation in a few areas of the liver sections from the mice treated with PBS and *Luc* mRNA@M-HNP, which was not observed in the liver sections from the *IL-10* mRNA@M-HNP treatment group (Figure S25). This finding is consistent with the slightly reduced plasma lipid levels associated with the *IL-10* mRNA@M-HNP treatment. No obvious injuries were observed in sections of the other organs among all treated groups. These combined data suggest that intravenous administration of *IL-10* mRNA@M-HNPs is safe at the examined dosage.

DISCUSSION

Atherosclerosis is considered a chronic inflammatory vascular disease, driven by complex cellular and molecular mechanisms. Recent advances in the mechanistic knowledge for atherogenesis reveal that the activation of inflammatory pathways in lesional macrophages is crucial throughout the complex progression of lesions in the artery wall.[7,36] Therefore, modulating inflammation by selectively activating or inhibiting specific signaling pathways in plaque macrophages represents a promising route for the management of atherosclerotic risk.

Upon binding to its receptor complex in macrophages, IL-10 activates JAK1/STAT3 signaling pathways and subsequently induces the production of the anti-inflammatory suppressor of cytokine signaling 3 (SOCS3).[37] Activation of IL-10 receptor signaling inhibits macrophage apoptosis by inducing the expression of cell-survival molecules, markedly suppresses the production of pro-inflammatory cytokines (TNF-α, IL-1β, IL-6, *etc.*), and enhances polarization of macrophages toward anti-inflammatory M2 phenotypes.[10] Additionally, IL-10 modulates lipid metabolism in macrophages by facilitating both cholesterol uptake and efflux.[38] It has been reported that patients with acute coronary syndrome (ACS) have significantly lower plasma levels of IL-10 than healthy controls,[39] and there is a negative correlation between IL-10 levels and future atherothrombotic events in survivors of myocardial infarction.[40,41] These clinical studies have indicated unequivocally the promising therapeutic role of IL-10 in the management of atherosclerosis. However, due to its intrinsic instability, IL-10 is systemically administered at high dosages to maintain the pharmacodynamic concentration, which may suppress immune response and increase the risk for infection.[42–44] To overcome the limitations mentioned above, the local expression of active IL-10 in atherosclerotic lesional macrophages may be an effective strategy to quell plaque inflammation and atherosclerosis.

This is a proof-of-concept study demonstrating that targeted mRNA delivery can produce the anti-inflammatory and immunoregulatory IL-10 protein specifically in plaque macrophages, resolving inflammation and thereby exerting antiather-

https://doi.org/10.1021/acsnano.3c00958
ACS Nano 2023, 17, 17721–17739

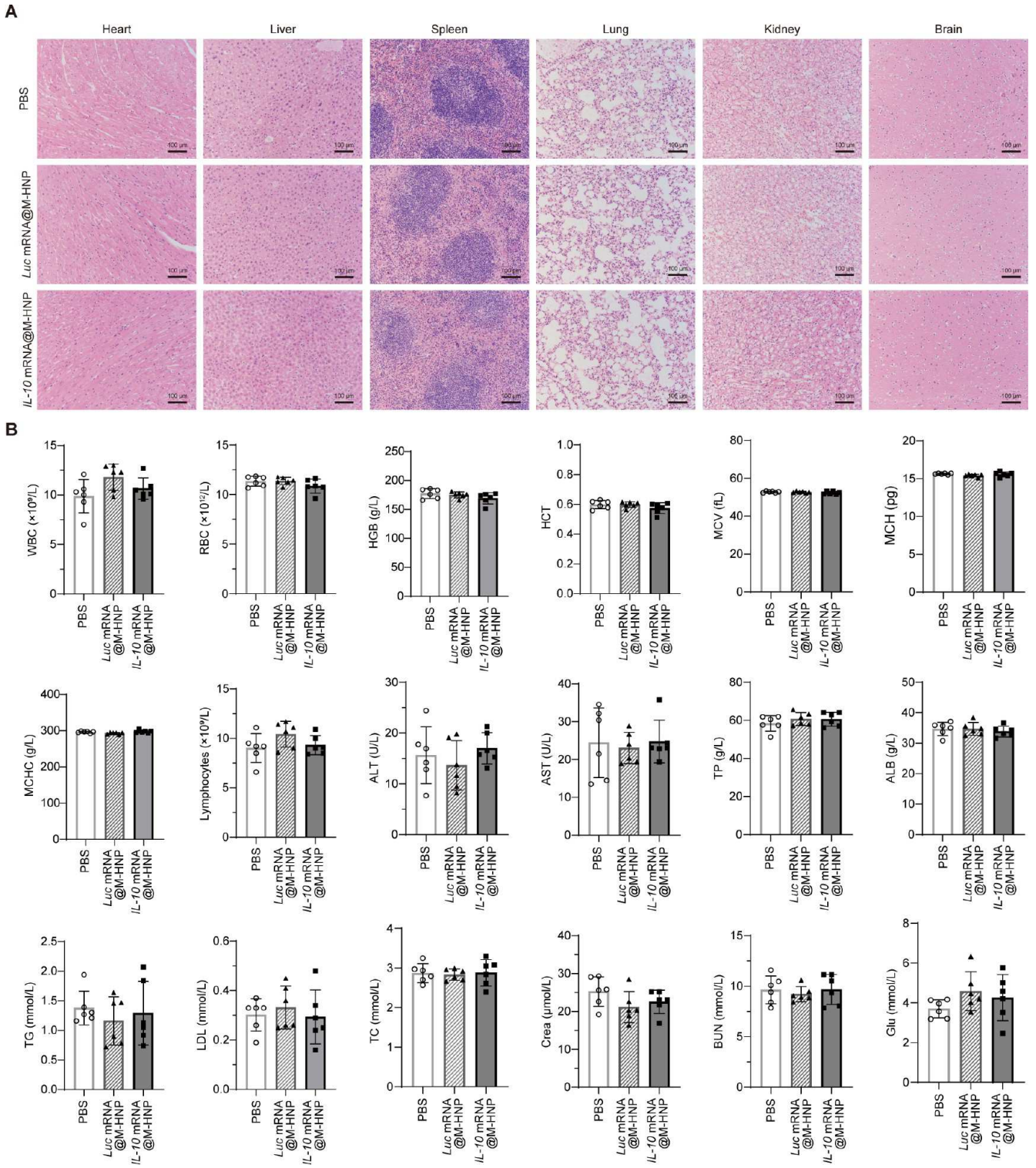

Figure 8. Safety evaluation in C57BL/6 mice. Healthy *C57BL/6* mice were injected with PBS, *Luc* mRNA@M-HNPs, or *IL-10* mRNA@M-HNPs twice per week for 4 weeks, and the indicated organs (A) and blood (B) were harvested on the third day after the last injection for the histological, hematological, and biochemical analyses. The organs were cross-sectioned and stained with H&E. Scale bars, 100 μm. The tested parameters in blood include RBC, WBC, HGB, HCT, MCV, MCH, MCHC, lymphocytes, ALT, AST, TP, ALB, TG, LDL, TC, Crea, BUN, and Clu, n = 6 mice per group. All data are shown as means ± SD. One-way ANOVA was performed to determine statistical significance, and there were no significant differences detected among the three groups.

osclerotic effects. Synthetic mRNAs have many advantages over therapeutic proteins, including (1) the well-established IVT manufacturing procedure that is cell-free, robust, scalable, and cost-effective and (2) the ability to produce any desired protein with intact structure, native glycosylation, and conformational properties inside the host cells.[45,46] Compared to DNAs and viral vectors previously employed in gene therapy, mRNAs only need to enter the cytoplasm rather than

https://doi.org/10.1021/acsnano.3c00958
ACS Nano 2023, 17, 17721−17739

the nucleus, which reduces the risk of insertional mutagenesis and lowers the cellular barriers for functional delivery.[47] mRNA technology has generated widespread interest in the biotechnology and pharmaceutical industry, especially since the rapid and successful clinical translation of SARS-CoV-2 mRNA vaccines.[48−50] Recent progress in the development of lipid NP (LNP) delivery systems is another major contributor to the clinical translation of RNA-based therapeutics and vaccines. The use of NP-formulated mRNA for vaccination, protein replacement therapy, and genome editing have cemented this as a robust platform technology that holds great potential to revolutionize the treatment of a wide range of diseases that are difficult to treat.[51−53] However, most of the systemically administered NP-formulated mRNAs, including lipid or lipid derivative NP formulations, accumulate primarily in the liver and spleen, which dramatically restricts the applicability of this nucleic acid modality to hepatic diseases.[47] It thus remains challenging to leverage this transformative technology to create effective drug products due to the lack of delivery strategies that enable the potent and specific transfer of mRNA to extrahepatic tissues.

In atherosclerotic lesions, macrophages, especially M2-like macrophages, are well-known as major producers of IL-10, providing multifactorial benefits including clearing apoptotic cells and debris by efferocytosis, facilitating tissue remodeling and regeneration through collagen formation, and altering lipid metabolism by generating pro-resolving lipid mediators.[54] M2 macrophages that are predominantly found in the fibrous cap surrounding the lipid core of plaques overexpress CD206 and are targets for the diagnosis and therapy of atherosclerosis.[54] Lymphoseek, the only FDA-approved lymphatic mapping agent, selectively targets macrophages through the specific binding of its mannose-based ligand and CD206 on the surface of macrophages.[55] To endow nanocarriers with both macrophage-targeting ability and high mRNA delivery efficiency, we designed a versatile NP platform composed of our previously reported cationic lipid G0-C14 and a mannose-modified PLGA-PEG copolymer. We incorporated clinically approved polymer building blocks (*e.g.*, PLGA, PEG or their derivatives) to endow NPs with versatile characteristics, such as multifunctional surface modifications, controlled release profiles, stability, and biocompatibility. Cationic G0-C14 was developed to effectively entrap mRNA and facilitate its endosomal escape, whereas PLGA-PEG-Mannose was incorporated as a biodegradable polymeric matrix to encapsulate mRNA, prolong the circulating lifetime, and facilitate cellular uptake by lesional macrophages. Unlike other previously reported atherosclerosis-related studies that focus on gene down-regulation strategies,[56,57] this present work is primarily focused on developing an mRNA-based nanotherapeutic approach for improved plaque stability by selectively delivering mRNA encoding inflammation-resolving factors within plaque lesions. To the best of our knowledge, NP-assisted targeted delivery of mRNA to lesional macrophages has seldom been explored for the treatment of atherosclerosis treatment.

Our results show that the developed *IL-10* mRNA@M-HNPs can be sufficiently internalized by M2-like macrophages through CD206-mediated interactions and efficiently induce IL-10 production. In a well-established WD-fed $Ldlr^{-/-}$ mouse model of atherosclerosis, we demonstrate the successful *in vivo* mRNA delivery to macrophage-rich plaques following iv injection of the targeted M-HNPs. Intriguingly, the data reveal that this approach can markedly inhibit the production of major pro-inflammatory cytokines, improve fibrous cap thickness, and decrease necrotic core area. The NP-mediated antiatherogenic benefit is most likely due to the resolution of inflammation through STAT3-dependent signaling and upregulated expression of cholesterol efflux-relative genes. Additionally, the safety profile of *IL-10* mRNA@M-HNPs was verified in both WD-fed $Ldlr^{-/-}$ mice and healthy *C57BL/6* mice, further demonstrating the promising translational potential of this targeted mRNA-based therapy for atherosclerosis.

Despite these encouraging results, additional investigations should be performed using different animal models (*e.g.*, humanized mouse models and nonhuman primates) that reflect pathologic features of human atherosclerosis at different disease stages to further validate this strategy for translational potential. Note that we developed a microfluidic-based method to prepare the hybrid NP formulation in this study. It is necessary to systemically study the scalability of this NP formulation method and develop a scalable manufacturing process that allows more controllable and reproducible mass production of such mRNA-NP systems, required for preclinical pharmacology and toxicology evaluation. It is worth noting that antiatherosclerotic effects of *IL-10* mRNA@M-HNPs could be further enhanced by administration in combination with other therapeutic or treatment modalities (*e.g.*, lipid-reducing therapies), which may improve the clinical translational potential of this inflammation-targeted mRNA therapy. The present study sheds light on an attractive concept: that mRNA can be transferred to a specific cell type in atherosclerotic plaques *via* this NP-platform, which can also be employed in delivering other types of RNA therapeutics (*e.g.*, microRNA, small interfering RNA, and their combinations), offering tremendous opportunities to explore and validate treatments for a broad range of cardiovascular diseases.

CONCLUSIONS

In summary, we developed a robust NP platform capable of delivering mRNA encoding IL-10 to plaque macrophages and investigated its therapeutic effects in a WD-fed $Ldlr^{-/-}$ mouse model of atherosclerosis as a proof-of-concept. This work shows enormous promise and demonstrates an encouraging step toward the clinical translation of inflammation-targeted therapies, potentially offering an effective therapeutic intervention for other related diseases.

EXPERIMENTAL SECTION

Preparation of Modified *IL-10* mRNA. *IL-10* mRNA was synthesized as described previously.[58] In brief, IL-10 Open Reading frame (ORF), 5′ untranslated region (UTR), and 3′ UTR sequences were constructed in the circular murine plasmid. mRNA templates were amplified from this plasmid using forward primers and reverse primers, including 120 poly(T) in PCR reactions. Templates were purified by the Universal DNA Purification and Recovery Kit (TIANGEN) and then examined by agarose gel electrophoresis (native agarose gel, 110 mV, 30 min). All mRNAs were *in vitro* transcribed by T7 RNA polymerase. Anti-Reverse Cap Analog (ARCA, APExBIO) and pseudouridine-5′-triphosphate (ΨTP; APExBIO) instead of uridine-5′-triphosphate (UTP) were added into this reaction. mRNA was purified using RNA Clean & Concentrator (Zymo Research) and analyzed by agarose gel electrophoresis (native agarose gel, 110 mV, 10 min). The fragment integrity of mRNA was analyzed by capillary electrophoresis (CE, QSep100 BiOptic Inc.). mRNA was quantified by NanoDrop 2000

https://doi.org/10.1021/acsnano.3c00958
ACS Nano 2023, 17, 17721−17739

spectrophotometer (Thermo Fisher Scientific) and stored at −80 °C for future use.

Synthesis of Polymers and Lipids. Copolymer PLGA-PEG-Mannose, Cy5.5-labeled PLGA-PEG (Cy5.5-PLGA-PEG), and PLGA-PEG were synthesized as described previously. In brief, tBOC-NH-PEG-NHS (0.2 g, 0.06 mM) was mixed with 4-aminophenyl α-D-mannopyranoside (MAN, 0.0195 g, 0.072 mM) and the reaction proceeded by catalysis by diisopropylethylamine (DIPEA, 103 μL, 0.6 mM) at room temperature (RT) for 12 h, followed by deprotection of BOC-protected amines by trifluoroacetic acid (TFA, 50 vol %) to obtain NH_2-PEG-Mannose. Cy5.5-PEG-NH_2 was synthesized by a Maleimide-Thiol click reaction where sulfo-Cy5.5-maleimide (5 mg, 0.072 mM) and NH_2-PEG-Thiol (0.014 g, 0.06 mM) were mixed and stirred in phosphate-buffered saline (PBS, pH = 7.0, 2 mL) accompanied by N_2 purging at RT for 48 h. PLGA-COOH (0.2 g, 5 μM) was transformed into PLGA-NHS by adding excessive *N*-hydroxysuccinimide (NHS, 5.7 mg, 0.05 mM) in the presence of 1-ethyl-3-(3-(dimethylamino)propyl)-carbodiimide (EDC, 10 mg, 0.05 mM). NH_2-PEG-Mannose, NH_2-PEG-Cy5.5, or NH_2-PEG-OCH_3 was added into PLGA-NHS and then reacted at RT for 48 h, accompanied by the catalyzation of DIPEA. The yielded PLGA-PEG-Mannose, Cy5.5-PLGA-PEG, and PLGA-PEG were precipitated in precool methanol/diethyl ether (50/50 v/v) and ultimately dried in a vacuum.

Cationic lipid compound G0-C14 was synthesized through a ring-opening reaction according to the method described previously,[59] while the molar ratio has been optimized. 1,2-epoxytetradecane was mixed with PAMAM dendrimer G0 at the molar ratio of 5:1 and stirred at 90 °C for 48 h. The products were characterized by ^{1}H NMR (400 MHz, chloroform-*d*), 3.63−3.51 (m, 5H), 3.47−3.12 (m, 10H), 2.81−2.19 (m, 36H), 1.53−1.13 (m, 110H), 0.86 (t, J = 6.8 Hz, 15H).

mRNA Complexation Ability of G0-C14. *EGFP* mRNA was complexed with G0-C14 at different weight ratios ranging from 1 to 90, and then mixtures were incubated at RT for 10 min. The samples were mixed with loading dye (Beyotime) and analyzed by electrophoresis in a 2% agarose gel running for 10 min at 110 V. The mRNA ladder was the double-stranded marker A (Sangon Biotech). Finally, the gel was imaged using a ChemiDoc system (Bio-Rad, USA).

Preparation of mRNA NPs. The mRNA NPs were formulated using a microfluidic device. In brief, copolymer (PLGA-PEG or PLGA-PEG-Mannose) and G0-C14 were dissolved in DMF at a weight ratio of 1:1, and the yielded solution was mixed with sodium acetate buffer (pH 4.6, 25 mM) containing mRNA by using the microfluidic system (Micro&Nano, China). The final weight ratio of three substances was 30:30:1 (copolymer: G0-C14: mRNA). The mixture was further dialyzed against PBS (10 mM, pH 7.4) for 2 h at 4 °C using cassettes with molecular weight cutoff of 3,500 MWCO (Thermo Fisher Scientific) to form stable mRNA NPs. Cy5.5-PLGA-PEG was incorporated into the preparation of NPs at 10% of the copolymer weight to form Cy5.5-labeled NPs used for cellular uptake and biodistribution studies. The size and zeta potential of mRNA NPs were measured by dynamic light scattering (DLS, Malvern, UK) and morphologies were characterized with a transmission electron microscope (TEM, Thermo Fisher Scientific, USA). mRNA encapsulation efficiencies of different NPs were determined by Quant-it RiboGreen RNA Assay kit (Thermo Fisher Scientific). NPs was mixed with 2% Triton X-100 for 2 min. A series of concentrations mRNA standard and NP samples were incubated with RiboGreen reagent for 5 min, and the fluorescence intensity was determined with a microplate reader (excitation/emission, 480/520 nm; Tecan, Switzerland).

mRNA NPs Stability Assessment. The capability of naked mRNA and mRNA encapsulated in NPs against FBS and RNase was tested and visualized by agarose gel electrophoresis. Briefly, 1 μg of naked *EGFP* mRNA or *EGFP* mRNA@M-HNPs was incubated with FBS (10%, v/v) or RNase A (10 ng/mL) at 37 °C at predetermined time points. The mRNA encapsulated in NPs was extracted with 50 mg/mL heparin sodium and was subjected to Gel-red-infused 2% agarose gel electrophoresis, followed by imaging by the ChemiDoc system. The NPs were incubated with PBS containing 10% FBS at 37 °C while being shaken (100 rpm) to mimic *in vivo* conditions. At predetermined time points, the particle size of the NPs solution in triplicate was analyzed by DLS, and the aggregation states of the NPs were measured using a microplate reader (Tecan, Switzerland) at 660 nm.

Cell Culture. BMDMs were isolated as described previously.[60] Briefly, C57BL/6J mice were euthanized with isoflurane, then femurs and tibias of hind legs were harvested and flushed by RPMI 1640 medium, and the suspensions were collected. The suspensions were passed over a 40 μm filter and treated with red blood cell lysate, followed by centrifuging at 500*g* for 5 min at 4 °C to harvest the cell pellet. The cells were cultured in RPMI 1640 complete medium with 20 ng/mL M-CSF (Peprotech) for 6−7 days and were employed in the indicated experiments. Human umbilical vein endothelial cells (HUVECs), NIH3T3, and RAW 264.7 cells were cultured in DMEM medium containing 10% FBS, 2 mM L-glutamine, and 100 units/mL penicillin and 100 mg/mL streptomycin, at 37 °C and in a humidified 5% CO_2 atmosphere.

Cellular Uptake Activity. BMDMs were seeded in 24-well plates (1×10^5 cells per well) overnight for adherence and then treated with 20 ng/mL IL-4 (PeproTech) for 48 h to obtain M2-like macrophages. Cells were incubated with Cy5.5-labeled NPs incorporated with the different percentages of mannose moiety (0%, 20%, 50%, and 100%) at a 0.5 μg/mL *IL-10* mRNA concentration for 4 h, and the fluorescence signals of these cells were detected by the BD LSRFortessa cell analyzer (BD Biosciences, USA).

BMDMs, HUVECs, and RAW 264.7 cells were inoculated at a density of 1×10^5 cells per well on 24-well plates overnight and then cultured in a complete medium containing 20 ng/mL IL-4 for 48 h. Cells were incubated with Cy5.5-labeled HNPs or M-HNPs at a 0.5 μg/mL *IL-10* mRNA concentration for 1, 2, 4, or 8 h, and the fluorescence signals of these cells were quantitatively analyzed by flow cytometry and were visualized at 4 h by confocal laser scanning microscope (CLSM). M2 macrophages were treated with a complete medium containing 1 mM mannan (CD206 receptor antagonist) for 30 min and were incubated with Cy5.5-labeled M-HNPs (0.5 μg/mL *IL-10* mRNA) for 1, 2, 4, or 8 h, and the fluorescence signals of these cells were analyzed by flow cytometry and CLSM.

mRNA NP *In Vitro* Transfection Activity. BMDMs and RAW 264.7 cells were respectively inoculated at the density of 1×10^5 cells on a 24-well plate and cultured in a complete medium for 12 h to attach. Cells were transfected with *EGFP* mRNA@M-HNPs at various mRNA concentrations (0.0625, 0.1250, 0.2500, and 0.5000 μg/mL) for 24 h. *EGFP* mRNA transfection with Lipofectamine 2000 reagent was performed according to the manufacturer's protocol as a positive control. To assess the transfection efficiency, cells were washed three times with PBS and harvested to measure the percentages of GFP-positive cells using flow cytometry, followed by histogram analysis by Flowjo software. CLSM was used to capture the fluorescence images of cells transfected with different formulations at 0.5 μg/mL *EGFP* mRNA.

Assessment of mRNA NPs Endosomal Escape. BMDMs were seeded in confocal dishes (Costar) at a density of 1×10^5 cells per well and cultured for 12 h. Cells were incubated with HNPs or M-HNPs incorporated with Cy5-labeled *Luc* mRNA at 0.5 μg/mL concentration for 4 h and were stained with Hoechst 33342 (Beyotime) and LysoTracker Green (Beyotime), and the fluorescence signals of these cells were analyzed by CLSM.

Western Blotting Assay. BMDMs (5×10^5 cells/well) were seeded in 6-well plates and then treated with fresh complete medium, *Luc* mRNA@M-HNPs (0.5 μg/mL), or *IL-10* mRNA@M-HNPs (0.5 μg/mL) for 24 h. The protein was extracted from these cells using RIPA lysis buffer supplemented with protease inhibitors (Beyotime). According to the manufacturer's instructions, total protein concentrations were determined by a BCA protein assay (Beyotime). The samples were separated by SDS−PAGE and then transferred to a poly(vinylidene fluoride) membrane (PVDF, Millipore). The PVDF membranes were blocked with 5% skim milk powder in TBST (50

https://doi.org/10.1021/acsnano.3c00958
ACS Nano 2023, 17, 17721−17739

mM Tris-HCl, pH 7.4 and 150 mM NaCl, and 0.1% Tween 20) for 1 h at rt and were incubated overnight with appropriate primary antibodies (anti-IL-10, anti-STAT3, anti-pSTAT3, anti-β-Action) at 4 °C. After incubating with secondary antibodies at room temperature for 1 h, the membranes were added to electrochemiluminescence (ECL) chromogenic substrate and the band images were acquired using a ChemiDoc imaging system (Bio-Rad, USA).

Cytotoxicity Evaluation. BMDMs, RAW 264.7 cells, and NIH3T3 cells were seeded into 96-well plates at a density of 2×10^4 cells per well and cultured overnight. Cells were treated with different mRNA concentrations (0.0625, 0.1250, 0.2500, 0.5000, and 1.0000 μg/mL) of *IL-10* mRNA@M-HNPs for 12 or 24 h. The cell viability was assessed using cell counting kit-8 (CCK-8) reagents (Beyotime). In brief, cells in each well were incubated with 10 μL of the CCK-8 solution for 2 h at 37 °C, and the absorbance at 450 nm was measured by a microplate reader.

Anti-inflammatory Effect *In Vitro*. BMDMs were inoculated with 2.5×10^5 cells per well in 12-well plates and maintained for 12 h. Cells were incubated with fresh medium or *IL-10* mRNA@M-HNPs (0.5 μg/mL) for 6 h and then stimulated with 500 ng/mL LPS for 24, 48, or 72 h. The total RNA was extracted using Trizol, and qRT-PCR was used to determine the gene levels of inflammatory cytokines including *IL-10*, *TNF-α*, *IL-1β*, and *IL-6*. The primers are summarized in Supplementary Table S3.

Antioxidative Stress Activity *In Vitro*. BMDMs were seeded at a density of 1×10^5 cells per well in 24-well plates for 12 h, incubated with fresh medium, *Luc* mRNA@M-HNP (0.5 μg/mL), or *IL-10* mRNA@M-HNPs (0.5 μg/mL) for 6 h, and then treated with 500 ng/mL LPS for 4 or 24 h. Untreated cells were used as the blank control. After incubation with 10 μM DCFH-DA in serum-free medium for 30 min, cells were rinsed three times with PBS and the intracellular fluorescence signal was measured by flow cytometry. The NO level was determined by the NO detection kit (Beyotime), and the *iNOS* expression level was detected by qRT-PCR. The *iNOS* primers are shown in Supplementary Table S3.

Antiapoptotic Activity in Macrophages. BMDMs were incubated with fresh medium, *Luc* mRNA@M-HNP (0.5 μg/mL), or *IL-10* mRNA@M-HNPs (0.5 μg/mL) for 6 h and then exposed to 200 μM H_2O_2 in fresh medium for 30 min. Untreated cells were used as the blank control. Cells were washed with PBS and stained with Calcein/PI apoptosis detection reagents (Beyotime) according to the manufacturer's protocol and the fluorescence signals were analyzed by fluorescence microscopy and flow cytometry.

The adherent BMDMs (1×10^5 cells per well) were treated with 80 μg/mL oxLDL (Yiyuanbiotech) for 24 h to obtain senescent foamy macrophages. The foam cells were treated with fresh medium, *Luc* mRNA@M-HNP (0.5 μg/mL), or *IL-10* mRNA@M-HNPs (0.5 μg/mL) for 24 h. The total RNAs were extracted with Trizol and the *AIM/CD5L*, *Bcl-2A1*, *MCL-1*, *PPAR-γ*, and *ABAC1* gene expression levels were evaluated by qRT-PCR. The primers are summarized in Supplementary Table 3.

Animals. C57BL/6J mice and male *Ldlr*$^{-/-}$ C57BL/6J mice (6−8 weeks old) were purchased from GemPharmatech Co., Ltd. The *Ldlr*$^{-/-}$ mice used in the atherosclerosis study have been described in previous studies.[61] In brief, a WD (D12079B, Research Diets) containing 22.6% protein, 45.4% carbohydrate, and 20% fat was fed to mice over 12 weeks to establish the atherosclerosis model in the *Ldlr*$^{-/-}$ mice. At study completion, the mice were anesthetized with isoflurane, and blood and tissue samples were collected and stored until further analysis.

Pharmacokinetic Study of NPs *In Vivo*. Wild-type C57BL/6J mice (n = 3) were intravenously injected with Cy5-*Luc* mRNA, Cy5-*Luc* mRNA@HNPs, and Cy5-*Luc* mRNA@M-HNPs at an mRNA dose of 15 μg per mouse. At predetermined time intervals (0, 0.5, 1, 2, 4, 8, 12, and 24 h), the whole blood samples with equal volume were collected into a 96-well blackboard and the fluorescence intensity of Cy5-mRNA was analyzed with an In-Vivo Imaging System (IVIS, PerkinElmer). Pharmacokinetic (PK) parameters were assessed by measuring the fluorescence intensity of Cy5-mRNA in blood at each time point and normalizing with the initial time point (0 h).

Biodistribution of Cy5.5-Labeled NPs in WD-fed *Ldlr*$^{-/-}$ Mice. 12-week WD-fed *Ldlr*$^{-/-}$ mice or healthy mice received intravenous injections of Cy5.5-labeled NPs at 15 μg *IL-10* mRNA per mouse. Mice injected with PBS were used as control. After 24 h, mice were anesthetized and perfused with 4% paraformaldehyde (PFA) in PBS, then the aorta, heart, liver, spleen, lung, and kidney were harvested and imaged using the IVIS. The imaging data were quantified by Living Image 4.5 software.

Atherosclerotic Lesions Analysis. 12-week WD-fed *Ldlr*$^{-/-}$ mice were intravenously injected with PBS, IL-10 protein (100 μg IL-10 protein/mouse), *Luc* mRNA@M-HNP (15 μg *Luc* mRNA/mouse), or *IL-10* mRNA@M-HNPs (15 μg *IL-10* mRNA/mouse) twice per week for 4 weeks, and WD-fed was also maintained in the treatment period. Mice were euthanized and perfused with cold 4% PFA in PBS on the third day after the last injection. The aorta and aortic root attached to the heart were fixed in 4% PFA, dehydrated, placed in an optical cutting temperature (OCT, Servicebio) compound, and preserved at −80 °C. Serial 10 μm sections of the brachiocephalic artery, aortic arch, and aortic root were obtained from frozen samples. For morphometric analysis, the whole aortas or the cross sections were stained with Oil Red O (ORO, Servicebio) to evaluate plaque areas, necrotic core size was analyzed with Harris's H&E staining, and cap thickness was assessed by collagen staining with picrosirius red (G-CLONE). Images were captured using a microscope (Olympus, USA) and quantified by ImageJ software.

Histology Analysis. The aortic roots of mice were analyzed by immunohistochemistry (IHC) and immunofluorescence. For IHC staining, the cross sections were pretreated with EDTA (pH 9.0) epitope retrieval solution for 20 min using a microwave, incubated with 3% hydrogen peroxide (Servicebio) for 25 min to block endogenous peroxidase, and blocked with 3% bovine serum albumin (BSA) in TBST for 30 min. The slides were treated with the primary antibody (anti-MMP9, anti-CD68, and anti-α-SMA) at 4 °C overnight and then stained using a diaminobenzidine peroxidase substrate kit (Impact DAB, Servicebio). For immunofluorescence analysis, the sections were blocked with 3% BSA for 30 min, incubated with anti-IL-10, anti-TNF-α, anti-IL-1β, anti-IL-6, anti-CD206, and anti-pSTAT3 primary antibody overnight at 4 °C, then treated with the fluorescent-labeled secondary antibody for 50 min at RT, and counterstained with DAPI for 5 min. Histological images were captured by a microscope (Olympus) or CLSM and were quantitatively analyzed using ImageJ software.

Determination of Inflammatory Cytokines in the Aorta and Serum. The aorta and serum were collected from the mice that received the indicated treatment. The aortas underwent homogenization in saline, followed by centrifugation. The supernatant was gathered to quantify the levels of IL-10 using ELISA kits (NeoBioscience). Similarly, the concentrations of IL-10, IL-1β, and IL-6 in the serum were determined by the ELISA assay.

Oxidative Stress Evaluation. Dihydroethidium (DHE, Beyotime) was used to detect superoxide anion generation in the aorta. Sections of the aortic root, aortic arch, and brachiocephalic artery were incubated with DHE (5 μM) in a light-protected humidified chamber at 37 °C for 30 min and counterstained with DAPI. CLSM was used to acquire the fluorescence images.

TUNEL Apoptosis Assay. TUNEL test (Servicebio) was applied to detect *in situ* cell death of the aortic root caused by DNA double-strand breaks. Cryosections of the aortic root were treated with proteinase K for 20 min at 37°C to thoroughly expose DNA. After three washes with PBS, the sections were incubated with terminal deoxynucleotidyl transferase (TdT) buffer for 1 h at 37°C, washed five times with PBS before air drying, and covered with antifade mount containing DAPI. Immunofluorescence images were acquired using CLSM and quantitively analyzed by ImageJ software.

Safety Evaluation. To measure potential *in vivo* toxicity, male C56BL/6 mice were treated long-term with PBS, *Luc* mRNA@M-HNPs, or *IL-10* mRNA@M-HNPs twice per week for 4 weeks. Body weight was recorded every day, and at the end of the experiment, the blood, heart, liver, spleen, lung, kidney, and brain in different treatment groups were collected. The organ coefficient was calculated

https://doi.org/10.1021/acsnano.3c00958
ACS Nano 2023, 17, 17721−17739

as the organ weight divided by the body weight. The heart, liver, spleen, lung, kidney, and brain were histologically assessed by H&E staining. Blood samples were analyzed for hematological and biochemical indicators, including RBC, WBC, HGB, HCT, MCV, MCH, MCHC, lymphocytes, ALT, AST, TP, ALB, TG, LDL, TC, Crea, BUN, and Clu.

Statistical Analysis. For statistics, Shapiro–Wilk and Kolmogorov–Smirnov normality tests were used to determine normality. Student's *t* test (two-tailed) or one-way analysis of variance (ANOVA) was used for multiple group comparisons when normal distribution was determined. Kruskal–Wall's test was used to calculate *P* values of non-normally distributed data. $P < 0.05$ was considered statistically significant. All statistics shown in the graphs were graded according to $*P < 0.05$, $**P < 0.01$, $***P < 0.001$, and $****P < 0.0001$. v8.2.1 GraphPad Prism 8 software was used for all statistical analyses.

ASSOCIATED CONTENT

Supporting Information

The Supporting Information is available free of charge at https://pubs.acs.org/doi/10.1021/acsnano.3c00958.

Figures S1 and S2: The characterization of PLGA-PEG-Mannose and G0-C14 by ^{1}H NMR spectra. Figure S3: Agarose gel electrophoresis assay. Figure S4: *In vitro* transcription (IVT) of *IL-10* mRNA. Figure S5–S15: The characterization, uptake, pharmacokinetics, biodistribution, transfection efficiency, endosomal escape, and cytotoxicity evaluation of NPs. Figure 16: ORO-staining of aortas from WD-fed $Ldlr^{-/-}$ mice. Figure S17: Levels of IL-10 in aortic tissues of WD-fed $Ldlr^{-/-}$ mice. Figure S18: Serum levels of IL-10, IL-1β, and IL-6. Figure S19: Oxidative stress assay. Figure S20: Histochemistry analysis of aortic root sections of NP-treated WD-fed $Ldlr^{-/-}$ mice. Figures S21 and S22: CD206 and pSTAT3 expression in aortic roots of NP-treated WD-fed $Ldlr^{-/-}$ mice. Figures S23–S25: *In vivo* safety evaluation of NPs. Table S1: *IL-10* mRNA sequences in this study. Table S2: Hematological analysis of WD-fed $Ldlr^{-/-}$ mice after administration. Table S3: Primer sequences of qRT-PCR. Table S4: Key resources table (PDF)

AUTHOR INFORMATION

Corresponding Authors

Xiaoyang Xu – *Department of Chemical and Materials Engineering and Department of Biomedical Engineering, New Jersey Institute of Technology, Newark, New Jersey 07102, United States;* orcid.org/0000-0002-1634-3329; Email: xiaoyang.xu@njit.edu

Xue-Qing Zhang – *Shanghai Frontiers Science Center of Drug Target Identification and Delivery, School of Pharmacy, National Key Laboratory of Innovative Immunotherapy, Shanghai Jiao Tong University, Shanghai 200240, PR China;* orcid.org/0000-0002-4954-2586; Email: xueqingzhang@sjtu.edu.cn

Authors

Mingzhu Gao – *Shanghai Frontiers Science Center of Drug Target Identification and Delivery, School of Pharmacy, National Key Laboratory of Innovative Immunotherapy, Shanghai Jiao Tong University, Shanghai 200240, PR China*

Maoping Tang – *Shanghai Frontiers Science Center of Drug Target Identification and Delivery, School of Pharmacy, National Key Laboratory of Innovative Immunotherapy, Shanghai Jiao Tong University, Shanghai 200240, PR China*

William Ho – *Department of Chemical and Materials Engineering, New Jersey Institute of Technology, Newark, New Jersey 07102, United States*

Yilong Teng – *Shanghai Frontiers Science Center of Drug Target Identification and Delivery, School of Pharmacy, National Key Laboratory of Innovative Immunotherapy, Shanghai Jiao Tong University, Shanghai 200240, PR China*

Qijing Chen – *Shanghai Frontiers Science Center of Drug Target Identification and Delivery, School of Pharmacy, National Key Laboratory of Innovative Immunotherapy, Shanghai Jiao Tong University, Shanghai 200240, PR China*

Lei Bu – *Leon H. Charney Division of Cardiology, Department of Medicine, NYU Grossman School of Medicine, New York, New York 10016, United States*

Complete contact information is available at: https://pubs.acs.org/10.1021/acsnano.3c00958

Author Contributions

X.-Q.Z., X.X., M.G., and L.B. conceived, designed, and directed the experiments. M.G. performed all the experiments and analyzed data. X.-Q.Z., X.X., M.G., and M.T. wrote the manuscript. Y.T. and Q.C. assisted with chemical synthesis and characterization. X.-Q.Z., X.X., M.G., M.T., and L.B. discussed results and provided conceptual advice. X.-Q.Z., X.X., M.G., W.H., and M.T. reviewed and edited the manuscript.

Notes

The authors declare no competing financial interest.

ACKNOWLEDGMENTS

This work was supported by the "Open Competition to Select the Best Candidates" Key Technology Program for Nucleic Acid Drugs of NCTIB (Grant No. NCTIB2022HS02002), the Natural Science Foundation of Shanghai (23ZR1427600), Shanghai Jiao Tong University Scientific and Technological Innovation Funds (2019TPA10), Foundation of National Facility for Translational Medicine (Shanghai) (TMSK-2020-008), the Interdisciplinary Program of Shanghai Jiao Tong University [project number ZH2018ZDA36 (19X190020006)], the National Science Foundation (2001606), and the Gustavus and Louise Pfeiffer Research Foundation Award.

REFERENCES

(1) Libby, P.; Buring, J. E.; Badimon, L.; Hansson, G. K.; Deanfield, J.; Bittencourt, M. S.; Tokgözoğlu, L.; Lewis, E. F. Atherosclerosis. *Nature Reviews Disease Primers* **2019**, *5* (1), 56.

(2) Charo, I. F.; Taub, R. Anti-inflammatory therapeutics for the treatment of atherosclerosis. *Nat. Rev. Drug Discovery* **2011**, *10* (5), 365–376.

(3) Roy, P.; Orecchioni, M.; Ley, K. How the immune system shapes atherosclerosis: roles of innate and adaptive immunity. *Nature Reviews Immunology* **2022**, *22* (4), 251–265.

(4) Bäck, M.; Yurdagul, A.; Tabas, I.; Öörni, K.; Kovanen, P. T. Inflammation and its resolution in atherosclerosis: mediators and therapeutic opportunities. *Nature Reviews Cardiology* **2019**, *16* (7), 389–406.

(5) Soehnlein, O.; Libby, P. Targeting inflammation in atherosclerosis - from experimental insights to the clinic. *Nat. Rev. Drug Discov* **2021**, *20* (8), 589–610.

(6) Moore, K.; Tabas, I. Macrophages in the pathogenesis of atherosclerosis. *Cell* **2011**, *145* (3), 341–355.

(7) Chen, W.; Schilperoort, M.; Cao, Y.; Shi, J.; Tabas, I.; Tao, W. Macrophage-targeted nanomedicine for the diagnosis and treatment of atherosclerosis. *Nature Reviews Cardiology* **2022**, *19* (4), 228–249.

(8) Murray, P. J.; Smale, S. T. Restraint of inflammatory signaling by interdependent strata of negative regulatory pathways. *Nat. Immunol* **2012**, *13* (10), 916−924.
(9) Kabat, A. M.; Pearce, E. J. Inflammation by way of macrophage metabolism. *Science* **2017**, *356* (6337), 488−489.
(10) Han, X.; Boisvert, W. A. Interleukin-10 protects against atherosclerosis by modulating multiple atherogenic macrophage function. *Thromb Haemost* **2015**, *113* (3), 505−512.
(11) Mattos, A.; de Jager-Krikken, A.; de Haan, M.; Beljaars, L.; Poelstra, K. PEGylation of interleukin-10 improves the pharmacokinetic profile and enhances the antifibrotic effectivity in CCl_4-induced fibrogenesis in mice. *J. Controlled Release* **2012**, *162* (1), 84−91.
(12) Donohue, J. H.; Rosenberg, S. A. The fate of interleukin-2 after in vivo administration. *J. Immunol* **1983**, *130* (5), 2203−2208.
(13) Huang, X.; Kong, N.; Zhang, X.; Cao, Y.; Langer, R.; Tao, W. The landscape of mRNA nanomedicine. *Nature Medicine* **2022**, *28* (11), 2273−2287.
(14) Rohner, E.; Yang, R.; Foo, K. S.; Goedel, A.; Chien, K. R. Unlocking the promise of mRNA therapeutics. *Nat. Biotechnol.* **2022**, *40* (11), 1586−1600.
(15) Dobrowolski, C.; Paunovska, K.; Hatit, M. Z. C.; Lokugamage, M. P.; Dahlman, J. E. Therapeutic RNA Delivery for COVID and Other Diseases. *Adv. Healthc Mater.* **2021**, *10* (15), No. e2002022.
(16) Han, X.; Mitchell, M. J.; Nie, G. Nanomaterials for Therapeutic RNA Delivery. *Matter* **2020**, *3* (6), 1948−1975.
(17) Hou, X.; Zaks, T.; Langer, R.; Dong, Y. Lipid nanoparticles for mRNA delivery. *Nature Reviews Materials* **2021**, *6*, 1078.
(18) Zhang, Y.; Sun, C.; Wang, C.; Jankovic, K. E.; Dong, Y. Lipids and Lipid Derivatives for RNA Delivery. *Chem. Rev.* **2021**, *121* (20), 12181−12277.
(19) Qiu, M.; Tang, Y.; Chen, J.; Muriph, R.; Ye, Z.; Huang, C.; Evans, J.; Henske, E. P.; Xu, Q. Lung-selective mRNA delivery of synthetic lipid nanoparticles for the treatment of pulmonary lymphangioleiomyomatosis. *Proc. Natl. Acad. Sci. U. S. A.* **2022**, *119* (8), No. e2116271119, DOI: 10.1073/pnas.2116271119.
(20) Rurik, J. G.; Tombácz, I.; Yadegari, A.; Méndez Fernández, P. O.; Shewale, S. V.; Li, L.; Kimura, T.; Soliman, O. Y.; Papp, T. E.; Tam, Y. K.; et al. CAR T cells produced in vivo to treat cardiac injury. *Science* **2022**, *375* (6576), 91−96.
(21) Xu, X.; Xie, K.; Zhang, X.-Q.; Pridgen, E. M.; Park, G. Y.; Cui, D. S.; Shi, J.; Wu, J.; Kantoff, P. W.; Lippard, S. J. Enhancing tumor cell response to chemotherapy through nanoparticle-mediated codelivery of siRNA and cisplatin prodrug. *Proc. Natl. Acad. Sci. U. S. A.* **2013**, *110* (46), 18638−18643.
(22) Chinetti-Gbaguidi, G.; Colin, S.; Staels, B. Macrophage subsets in atherosclerosis. *Nature Reviews Cardiology* **2015**, *12* (1), 10−17.
(23) Varasteh, Z.; Mohanta, S.; Li, Y.; López Armbruster, N.; Braeuer, M.; Nekolla, S. G.; Habenicht, A.; Sager, H. B.; Raes, G.; Weber, W.; et al. Targeting mannose receptor expression on macrophages in atherosclerotic plaques of apolipoprotein E-knockout mice using (68)Ga-NOTA-anti-MMR nanobody: non-invasive imaging of atherosclerotic plaques. *EJNMMI Res.* **2019**, *9* (1), 5.
(24) Yu, T.; Gan, S.; Zhu, Q.; Dai, D.; Li, N.; Wang, H.; Chen, X.; Hou, D.; Wang, Y.; Pan, Q.; et al. Modulation of M2 macrophage polarization by the crosstalk between Stat6 and Trim24. *Nat. Commun.* **2019**, *10* (1), 4353.
(25) Luiz, J. P. M.; Toller-Kawahisa, J. E.; Viacava, P. R.; Nascimento, D. C.; Pereira, P. T.; Saraiva, A. L.; Prado, D. S.; LeBert, M.; Giurisato, E.; Tournier, C.; et al. MEK5/ERK5 signaling mediates IL-4-induced M2 macrophage differentiation through regulation of c-Myc expression. *J. Leukoc Biol.* **2020**, *108* (4), 1215−1223.
(26) Poon, W.; Kingston, B. R.; Ouyang, B.; Ngo, W.; Chan, W. C. W. A framework for designing delivery systems. *Nat. Nanotechnol* **2020**, *15* (10), 819−829.
(27) Li, J.; Jiang, X.; Li, H.; Gelinsky, M.; Gu, Z. Tailoring Materials for Modulation of Macrophage Fate. *Adv. Mater.* **2021**, *33* (12), No. e2004172.
(28) Tabas, I. Macrophage death and defective inflammation resolution in atherosclerosis. *Nature Reviews Immunology* **2010**, *10* (1), 36−46.
(29) Kong, P.; Cui, Z.-Y.; Huang, X.-F.; Zhang, D.-D.; Guo, R.-J.; Han, M. Inflammation and atherosclerosis: signaling pathways and therapeutic intervention. *Signal Transduction and Targeted Therapy* **2022**, *7* (1), 131.
(30) Yang, S.; Lian, G. ROS and diseases: role in metabolism and energy supply. *Mol. Cell. Biochem.* **2020**, *467* (1−2), 1−12.
(31) Zhou, Z.; Ni, K.; Deng, H.; Chen, X. Dancing with reactive oxygen species generation and elimination in nanotheranostics for disease treatment. *Adv. Drug Delivery Rev.* **2020**, *158*, 73−90.
(32) Pacher, P.; Beckman, J. S.; Liaudet, L. Nitric oxide and peroxynitrite in health and disease. *Physiol Rev.* **2007**, *87* (1), 315−424.
(33) Morrell; C, N. Reactive oxygen species: finding the right balance. *Circ. Res.* **2008**, *103* (6), 571−572.
(34) Ezhov, M.; Safarova, M.; Afanasieva, O.; Mitroshkin, M.; Matchin, Y.; Pokrovsky, S. Matrix Metalloproteinase 9 as a Predictor of Coronary Atherosclerotic Plaque Instability in Stable Coronary Heart Disease Patients with Elevated Lipoprotein(a) Levels. *Biomolecules* **2019**, *9* (4), 129.
(35) Wågsäter, D.; Zhu, C.; Björkegren, J.; Skogsberg, J.; Eriksson, P. MMP-2 and MMP-9 are prominent matrix metalloproteinases during atherosclerosis development in the Ldlr(−/−)Apob(100/100) mouse. *Int. J. Mol. Med.* **2011**, *28* (2), 247−253.
(36) Tabas, I.; Lichtman, A. H. Monocyte-Macrophages and T Cells in Atherosclerosis. *Immunity* **2017**, *47* (4), 621−634.
(37) Mosser, D. M.; Zhang, X. Interleukin-10: new perspectives on an old cytokine. *Immunol Rev.* **2008**, *226*, 205−218.
(38) Han, X.; Kitamoto, S.; Wang, H.; Boisvert, W. A. Interleukin-10 overexpression in macrophages suppresses atherosclerosis in hyperlipidemic mice. *Faseb j* **2010**, *24* (8), 2869−2880.
(39) Barcelos, A. L. V.; de Oliveira, E. A.; Haute, G. V.; Costa, B. P.; Pedrazza, L.; Donadio, M. V. F.; de Oliveira, J. R.; Bodanese, L. C. Association of IL-10 to coronary disease severity in patients with metabolic syndrome. *Clin. Chim. Acta* **2019**, *495*, 394−398.
(40) Seljeflot, I.; Hurlen, M.; Solheim, S.; Arnesen, H. Serum levels of interleukin-10 are inversely related to future events in patients with acute myocardial infarction. *J. Thromb Haemost* **2004**, *2* (2), 346−379.
(41) Cavusoglu, E.; Marmur, J. D.; Hojjati, M. R.; Chopra, V.; Butala, M.; Subnani, R.; Huda, M. S.; Yanamadala, S.; Ruwende, C.; Eng, C.; et al. Plasma interleukin-10 levels and adverse outcomes in acute coronary syndrome. *Am. J. Med.* **2011**, *124* (8), 724−730.
(42) Minshawi, F.; Lanvermann, S.; McKenzie, E.; Jeffery, R.; Couper, K.; Papoutsopoulou, S.; Roers, A.; Muller, W. The Generation of an Engineered Interleukin-10 Protein With Improved Stability and Biological Function. *Front Immunol* **2020**, *11*, 1794.
(43) Sathish, J. G.; Sethu, S.; Bielsky, M. C.; de Haan, L.; French, N. S.; Govindappa, K.; Green, J.; Griffiths, C. E.; Holgate, S.; Jones, D.; et al. Challenges and approaches for the development of safer immunomodulatory biologics. *Nat. Rev. Drug Discov* **2013**, *12* (4), 306−324.
(44) Terkeltaub, R. A. IL-10: An "immunologic scalpel" for atherosclerosis? *Arterioscler Thromb Vasc Biol.* **1999**, *19* (12), 2823−2825.
(45) Kowalski, P. S.; Rudra, A.; Miao, L.; Anderson, D. G. Delivering the Messenger: Advances in Technologies for Therapeutic mRNA Delivery. *Mol. Ther* **2019**, *27* (4), 710−728.
(46) Buschmann, M. D.; Carrasco, M. J.; Alishetty, S.; Paige, M.; Alameh, M. G.; Weissman, D. Nanomaterial Delivery Systems for mRNA Vaccines. *Vaccines (Basel)* **2021**, *9* (1), 65.
(47) Hajj, K. A.; Whitehead, K. A. Tools for translation: non-viral materials for therapeutic mRNA delivery. *Nature Reviews Materials* **2017**, *2* (10), 17056.
(48) Chaudhary, N.; Weissman, D.; Whitehead, K. A. mRNA vaccines for infectious diseases: principles, delivery and clinical translation. *Nat. Rev. Drug Discovery* **2021**, *20*, 817.

(49) Li, B.; Luo, X.; Dong, Y. Effects of Chemically Modified Messenger RNA on Protein Expression. *Bioconjug Chem.* **2016**, *27* (3), 849−853.
(50) Pardi, N.; Hogan, M. J.; Porter, F. W.; Weissman, D. mRNA vaccines — a new era in vaccinology. *Nat. Rev. Drug Discovery* **2018**, *17* (4), 261−279.
(51) Ledford, H. Moderna COVID vaccine becomes second to get US authorization. *Nature* **2020**, DOI: 10.1038/d41586-020-03593-7.
(52) Collén, A.; Bergenhem, N.; Carlsson, L.; Chien, K. R.; Hoge, S.; Gan, L.-M.; Fritsche-Danielson, R. VEGFA mRNA for regenerative treatment of heart failure. *Nat. Rev. Drug Discovery* **2022**, *21* (1), 79−80.
(53) Wei, T.; Cheng, Q.; Farbiak, L.; Anderson, D. G.; Langer, R.; Siegwart, D. J. Delivery of Tissue-Targeted Scalpels: Opportunities and Challenges for In Vivo CRISPR/Cas-Based Genome Editing. *ACS Nano* **2020**, *14* (8), 9243−9262.
(54) Bi, Y.; Chen, J.; Hu, F.; Liu, J.; Li, M.; Zhao, L. M2Macrophages as a Potential Target for Antiatherosclerosis Treatment. *Neural Plast* **2019**, *2019*, No. 6724903.
(55) Surasi, D. S.; O'Malley, J.; Bhambhvani, P. 99mTc-Tilmanocept: A Novel Molecular Agent for Lymphatic Mapping and Sentinel Lymph Node Localization. *J. Nucl. Med. Technol.* **2015**, *43* (2), 87−91.
(56) Huang, X.; Liu, C.; Kong, N.; Xiao, Y.; Yurdagul, A., Jr; Tabas, I.; Tao, W. Synthesis of siRNA nanoparticles to silence plaque-destabilizing gene in atherosclerotic lesional macrophages. *Nat. Protoc* **2022**, *17* (3), 748−780.
(57) Bai, Q.; Xiao, Y.; Hong, H.; Cao, X.; Zhang, L.; Han, R.; Lee, L. K. C.; Xue, E. Y.; Tian, X. Y.; Choi, C. H. J. Scavenger receptor-targeted plaque delivery of microRNA-coated nanoparticles for alleviating atherosclerosis. *Proc. Natl. Acad. Sci. U. S. A.* **2022**, *119* (39), No. e2201443119.
(58) Zeng, C.; Hou, X.; Yan, J.; Zhang, C.; Li, W.; Zhao, W.; Du, S.; Dong, Y. Leveraging mRNA Sequences and Nanoparticles to Deliver SARS-CoV-2 Antigens In Vivo. *Adv. Mater.* **2020**, *32* (40), No. e2004452.
(59) Bai, X.; Zhao, G.; Chen, Q.; Li, Z.; Gao, M.; Ho, W.; Xu, X.; Zhang, X.-Q. Inhaled siRNA nanoparticles targeting IL11 inhibit lung fibrosis and improve pulmonary function post-bleomycin challenge. *Science Advances* **2022**, *8* (25), No. eabn7162.
(60) Tao, W.; Yurdagul, A., Jr.; Kong, N.; Li, W.; Wang, X.; Doran, A. C.; Feng, C.; Wang, J.; Islam, M. A.; Farokhzad, O. C.; et al. siRNA nanoparticles targeting CaMKIIγ in lesional macrophages improve atherosclerotic plaque stability in mice. *Sci. Transl Med.* **2020**, *12* (553). DOI: 10.1126/scitranslmed.aay1063.
(61) Zhang, X. Q.; Even-Or, O.; Xu, X.; van Rosmalen, M.; Lim, L.; Gadde, S.; Farokhzad, O. C.; Fisher, E. A. Nanoparticles containing a liver X receptor agonist inhibit inflammation and atherosclerosis. *Adv. Healthc Mater.* **2015**, *4* (2), 228−236.

https://doi.org/10.1021/acsnano.3c00958
ACS Nano 2023, 17, 17721−17739